DYNAMICAL LOW-RANK INTEGRATOR FOR THE LINEAR BOLTZMANN EQUATION: ERROR ANALYSIS IN THE DIFFUSION LIMIT*

ZHIYAN DING[†], LUKAS EINKEMMER[‡], AND QIN LI[§]

Abstract. Dynamical low-rank algorithms are a class of numerical methods that compute lowrank approximations of dynamical systems. This is accomplished by projecting the dynamics onto a low-dimensional manifold and writing the solution directly in terms of the low-rank factors. The approach has been successfully applied to many types of differential equations. Recently, efficient dynamical low-rank algorithms have been proposed in [L. Einkemmer, A Low-Rank Algorithm for Weakly Compressible Flow, arXiv:1804.04561, 2018; L. Einkemmer and C. Lubich, SIAM J. Sci. Comput., 40 (2018), pp. B1330-B1360] to treat kinetic equations, including the Vlasov-Poisson and the Boltzmann equation. There it was demonstrated that the methods are able to capture the lowrank structure of the solution and significantly reduce numerical cost, while often maintaining high accuracy. However, no numerical analysis is currently available. In this paper, we perform an error analysis for a dynamical low-rank algorithm applied to the multiscale linear Boltzmann equation (a classical model in kinetic theory) to showcase the validity of the application of dynamical lowrank algorithms to kinetic theory. The equation, in its parabolic regime, is known to be rank 1 theoretically, and we will prove that the scheme can dynamically and automatically capture this low-rank structure. This work thus serves as the first mathematical error analysis for a dynamical low-rank approximation applied to a kinetic problem.

 $\textbf{Key words.} \ \ \text{dynamical low-rank approximation, multiscale analysis, linear Boltzmann equation, low-rank structure}$

AMS subject classifications. 65F55, 35L02, 65M06, 80A21

DOI. 10.1137/20M1380788

1. Introduction. Kinetic equations are a class of model equations used to describe the statistical behavior of a large number of particles that follow the same physical laws. They have been widely used in many aspects of physics and engineering. These equations, despite having different terms for various specific kinds of particles, share a similar structure: The dynamics is described in phase space and the solution is thus a distribution function u(t, x, v) that counts the density of particles at a particular time t, location x, and velocity v. One main challenge for the computation of kinetic equation comes from the fact that the equation is supported on phase space instead of physical space, and thus the dimensionality of the problem typically doubles.

During the past decade, numerous methods have been proposed to numerically solve kinetic equations and many of them succeed in reducing computational cost

^{*}Received by the editors November 23, 2020; accepted for publication (in revised form) May 20, 2021; published electronically August 19, 2021.

https://doi.org/10.1137/20M1380788

Funding: The work of the first author was partially supported by the Wisconsin Data Science Initiative and National Science Foundation grants DMS-1750488 and TRIPODS: 1740707. The work of the third author was partially supported by National Science Foundation grants DMS-1619778 and RNMS KI-NET 1107291.

 $^{^\}dagger Department$ of Mathematics, University of Wisconsin–Madison, Madison, WI 53706 USA (zding49@wisc.edu).

 $^{^{\}ddagger} Department$ of Mathematics, University of Innsbruck, Innsbruck, Austria (lukas.einkemmer@uibk.ac.at).

[§]Department of Mathematics and Wisconsin Institute for Discovery, University of Wisconsin–Madison, Madison, WI 53706 USA (qinli@math.wisc.edu).

without sacrificing accuracy. The main body of work concentrates on developing fast solvers for the collision operators and overcoming the stability requirement of the time discretization [24, 22], through either finding fast methods to treat the transport term [17, 48, 5, 12] or implementing the resulting discrete system efficiently [18, 13]. However, reducing the complexity due to the high dimensionality is largely left unaddressed. The difficulty here is rather clear. To compute PDEs, one needs to sample a certain amount of discrete points per dimension, and for kinetic equations that have high dimensionality, the degrees of freedom are large, driving up the numerical cost.

The viewpoint of degrees of freedom merely depending on the dimensionality of the problem was challenged in recent years; see [45] and references therein. In these works, the traditional approach is abandoned and one explores the structure of the intrinsic low-dimensional manifold where the PDE solution lives on. The method is designed to follow the flow of the dynamics and to identify the important features in the evolution. Since the equation is projected onto a solution manifold of lower dimensionality, only the core information is preserved and redundant information is neglected. The numerical cost thus depends mainly on the intrinsic dimensionality of the dynamics, rather than the total number of discrete points. The method was first utilized to deal with coupled ODE systems [38] and then was applied to a range of problems for which its accuracy has been demonstrated.

The success in dealing with ODE systems inspired the generalization to PDEs. More recently, a class of efficient numerical schemes were proposed for computing kinetic equations, including the radiative transfer equation [47], the Vlasov–Poisson system [28, 14], the Vlasov–Maxwell system [16], and the classical Boltzmann equation [11] in both collisionless and strong-collisional regimes. In these experiments, it was observed that both the sophisticated Landau damping phenomenon for the Vlasov–Poisson system [49, 44], and the incompressible Navier–Stokes limit for the Boltzmann equation are captured rather accurately at very low cost. Different equations may require slightly modified dynamical low-rank algorithms to suit the specific structures of the equation, but the general approach is quite similar. The main features in the evolution are preserved by following the flow of the equation projected onto the low-dimensional solution manifold.

However, despite the strong intuition and the many promising numerical experiments, rigorous mathematical analysis is largely absent, especially in the PDE setting. There are two major difficulties, one from the theoretical level and one numerical. First, we often do not have results to show that the true solution is indeed approximately of low-rank. This point is more subtle than one might think. In fact, a Fourier expansion is also a low-rank approximation. But, a Fourier expansion uses a fixed set of basis functions, and the prediction of the rank is higher than the intrinsic rank of the solution. In addition, showing the low-rank structure by performing a Fourier decomposition relies on assuming smoothness of the solution, which for kinetic equations is certainly problematic. It should be noted, however, that for elliptic equations some results can be obtained [6].

The second difficulty is numerical: How to show the method can capture the low-rank structure of the solution? For the ODE case an analysis has been performed in [26] and related works, but this analysis applies only to the nonstiff case and is thus not applicable to PDEs. The only mathematical analysis of a dynamical low-rank scheme in the PDE setting we are aware of is found in [46]. This paper considers a special situation where the stiffness originates only from the linear differential operator whose corresponding flow is exactly computable within the low-rank formulation. This separation suggests a splitting procedure that decouples the stiff and nonstiff

dynamics, which permits a convergence analysis of the resulting method. This is not the situation for kinetic equations, and thus the analysis does not apply.

In this paper, we will consider a multiscale linear Boltzmann equation. The equation is equipped with a parameter called the Knudsen number, and when it is small, the equation has a strong collision operator and is in the diffusive scaling. It is a well-known result that when this happens, the solution reduces to a rank-1 function, namely the solution can be written as a multiplication of two functions, one for x and one for v, respectively. The first challenge mentioned above therefore turns out to be trivial in this case. In this particular paper, we aim at solving the second challenge, which is to prove the dynamical low-rank algorithm can indeed capture this low-rank structure. More specifically, we will show, through utilizing the Hilbert expansion, that in the small Knudsen number limit, the method automatically captures the rank-1 behavior of the solution. These results imply that compared to the traditional approaches that require discretization of the full phase space, the essential degrees of freedom only scale as the number of grid points in physical space.

We should mention that the results shown here only address the low-rank dynamics of the linear Boltzmann equation. It is a showcase for the validity of the algorithm on kinetic equations and serves as a stepping stone for future studies on more complicated kinetic equations. We also stress that although the linear Boltzmann equation itself is linear, the studied dynamical low-rank algorithm is nonlinear and involved, making the proof highly nontrivial. We report the analytical result showing the performance of different time integrators, discussing both advantages and disadvantages in the asymptotic regimes.

1.1. Multiscale linear Boltzmann equation. We first give a quick overview of the equation. In d > 1 dimension, letting $(t, x, v) \in \mathbb{R}^+ \times \Omega_x \times \mathcal{S}^{d-1}$, the equation reads

(1.1)
$$\partial_t u(t, x, v) = \mathcal{L}u = -\frac{v}{\epsilon} \cdot \nabla_x u(t, x, v) + \frac{\sigma(x)}{\epsilon^2} \left(\rho(x) - u(t, x, v)\right),$$

where $\sigma(x)$ is the scattering cross section, $\Omega_x \subset \mathbb{R}^d$, ϵ is called the Knudsen number, which represents the ratio between the mean free path and the typical domain length, and v is the angular variable. Since $v \in \mathcal{S}^{d-1}$, the unit sphere in d dimensional space, all v have the same amplitude. The density ρ is defined as follows:

(1.2)
$$\rho(x) = \langle u(t, x, v) \rangle_v = \frac{1}{|\mathcal{S}^{d-1}|} \int_{\mathcal{S}^{d-1}} u(t, x, v) \, \mathrm{d}v \,,$$

where $|\mathcal{S}^{d-1}|$ is the volume of \mathcal{S}^{d-1} and $\langle \cdot \rangle_v$ denotes the average with respect to $v \in \mathcal{S}^{d-1}$. For the sake of convenience we shorten the notation

$$\mathrm{d}\mu_v = \frac{1}{|\mathcal{S}^{d-1}|} \, \mathrm{d}v \,,$$

where $d\mu_v$ is the normalized measure in $v \in \mathcal{S}^{d-1}$. The equation is written in diffusion scaling, meaning the transport term $v \cdot \nabla_x u$ and the collision term $\rho - u$ are enlarged by $\frac{1}{\epsilon}$ and $\frac{1}{\epsilon^2}$, respectively.

It is a well-known result that when $\epsilon \to 0$, the solution u of (1.1) will asymptotically approach ρ and thus becomes v independent. Furthermore, ρ solves the heat equation, with C_d being a constant that depends on d only:

(1.3)
$$\partial_t \rho = \nabla_x \cdot \left(\frac{1}{C_d \sigma(x)} \nabla_x \rho \right) , \quad (t, x) \in \mathbb{R}^+ \times \Omega_x .$$

For this reason, this is termed the parabolic regime, and the limit is called the diffusion limit. For this paper, this limit is particularly interesting because it essentially shows that $u(t, x, v) \sim \rho(t, x)$ is approximately of rank 1.

There are two difficulties in computing this equation. First, when the Knudsen number ϵ is small, both the transport term and the collision operator are stiff. A traditional numerical method would require small time step size that resolves the stiffness. Second, (1.1) is posed in a 2d-1 dimensional phase space. Suppose the equation has N_x grid points per spatial direction and N_v grid points per velocity direction; then $N_x^d N_v^{d-1}$ floating point numbers are needed. The large increase in the degrees of freedom is usually referred to as the curse of dimensionality in the literature.

There are indeed techniques developed to enlarge the stability region to overcome the stiffness problem as mentioned in the first challenge. In the kinetic framework, it is usually referred to as asymptotic preserving [21, 7, 30, 3, 9, 34, 8, 29]. Also see reviews [20, 23, 10]. However, the investigation into the second problem is mostly open. The belief that numerical cost mostly depends on the number of grid points and thus the degrees of freedom has been firm and essentially has not been challenged in the literature till the proposal of the dynamical low-rank approximation.

1.2. Dynamical low-rank approximation. Dynamical low-rank approximation is a systematic approach to tackling the curse of dimensionality for time-dependent problems. Believing that the number of grid points usually overrepresents the necessary numerical information, the main aim of the approximation is to explore the rank structure of the solution manifold. Instead of seeking the solution on a fixed set of grid points, the method evolves the low-rank representation and characterizes the flow of the solution on a low-dimensional manifold.

There are many ways to decompose the solution into its low-rank presentation. For kinetic equations in particular, it is rather straightforward to separate the physical space and the velocity space,

(1.4)
$$u(t,x,v) = \sum_{i,j=1}^{r} S_{i,j} X_i(t,x) V_j(t,v),$$

so that the low-rank factors X_i and V_j depend only on either x or v, respectively. In the formula, r is the rank and is typically significantly smaller than $\min(N_x, N_v)$. For this presentation, the number of degrees of freedom is $O(r(N_x^d + N_v^{d-1}))$.

Historically, dynamical low-rank approximations have been considered extensively in high-dimensional problems arising in quantum mechanics. Finding a low-rank approximation there makes the computation tractable; see [43, 42] and [36, 37, 4] for a mathematical treatment. The application of the method in a general setting is studied in [26, 27, 40, 1], where both the matrix and the general tensor formats are investigated. In the initial development, one significant disadvantage was observed: the methods are not robust with respect to overapproximation. Several strategies were proposed to address the issue, including both regularization and the projector splitting integrator. The latter is viewed as a major improvement [38] in enhancing the robustness with respect to small singular values [25]. This approach was later extended to various tensor formats [37, 39, 19, 41] and is the approach to be utilized in this paper.

The application of dynamical low-rank approximation for kinetic equations is relatively recent. Numerical experiments have been performed on the Vlasov–Poisson

[14, 15], the Vlasov–Maxwell [16], and the Boltzmann equation [11], and the numerical evidence is very promising. However, theoretical justification have been lacking.

In particular, from a mathematical point of view we need to answer two questions:

- 1. When do the solutions have low-rank structures?
- 2. Can dynamical low-rank approximation capture this structure?

The first question, in the kinetic framework, would be addressed by utilizing the fluid limit justification, as shown in (1.1) and (1.3). Since one can show that as $\epsilon \to 0$ we get $u(t, x, v) = \rho(t, x)$, the velocity direction completely degenerates, and the rank of the representation in (1.4) is simply 1. It is then reasonable to expect that for small ϵ the solution is only slightly different from its rank-1 approximation.

Addressing the second question relies on proper algorithm design. As mentioned above, we will use the projector splitting approach. This leads to a set of three evolution equations for S, X, and V, respectively, and all three will be advanced in every single time step in a proper order. It turns out that the specific time integrator for each equation plays a crucial role. More specifically, we will show that the implicit Euler method, due to the lack of symmetry, requires fine time discretization for capturing the rank structure, while the Crank–Nicolson implicit Euler (CNIE) method will converge with very relaxed constraints on the time step size but does require well-prepared initial data. Note that in the CNIE method we use the Crank–Nicolson scheme for X and S and the implicit Euler scheme for V. We propose to use the implicit Euler method for the initial step and a very small time step size, to reveal the structure of the PDE solution, and then switch to CNIE to preserve this structure.

The rest of the paper is organized as follows. In section 2 we present the application of the dynamical low-rank projector splitting integrator to the linear Boltzmann equation. Both the semi discrete splitting scheme and the fully discrete methods are presented, in sections 2.1 and 2.2, respectively. In section 3 we state and prove the main results. In section 3.1 we study the numerical cost saving, and an intuitive explanation of the error analysis is presented in section 3.2. Sections 3.3 and 3.4 are dedicated to the error analysis with the implicit Euler and CNIE time integrator, respectively, and we summarize the analysis with a final proposal of an algorithm in section 3.5. Some parts of the proof in section 3 are rather tedious, and we leave them to the appendix. Numerical evidence is presented in section 4.

2. Numerical scheme. We present the application of the dynamical low-rank approximation method to the linear Boltzmann equation in this section. We follow the framework and notations in [14]. Throughout the paper we use the standard L^2 vector space in both the spatial and the velocity domain. That is, we have

$$\langle f, g \rangle_x = \int f(x)g(x) dx, \quad \langle f, g \rangle_v = \int f(v)g(v) d\mu_v.$$

We call a function f(x, v) a rank-r function if it can be expanded by a set of r orthonormal basis functions in x and v. All these functions are collected to the set \mathcal{M} .

DEFINITION 2.1 (rank-r function in $L_2(dx dv)$). The collection of all rank-r functions is denoted by

$$\mathcal{M} = \left\{ f(x, v) \in L^2\left(\Omega_x \times \mathcal{S}^{d-1}\right) : f(x, v) \text{ is rank-r} \right\},$$

where f(x,v) is rank-r, meaning $f(x,v) = \sum_{i,j=1}^r S_{i,j} X_i(x) V_j(v)$, where X_i and V_i where orthonormal in physical and velocity space, respectively:

$$\langle X_i, X_j \rangle_x = \int_{\Omega_x} X_i X_j \, \mathrm{d}x = \delta_{ij}, \quad \langle V_i, V_j \rangle_v = \int_{\mathcal{S}^{d-1}} V_i V_j \, \mathrm{d}\mu_v = \delta_{ij}.$$

We note that in this definition, only the rank, r, is fixed. The basis functions X_i and V_j can be arbitrary, as long as the orthogonality condition is satisfied. We further emphasize that \mathcal{M} is not a function space; it is easily seen that the summation of two rank-r functions may not be rank-r.

It is unlikely that the solution is of rank-r, i.e., in \mathcal{M} , for all time. However, numerically one can argue that the solution is approximately of low rank. Thus for the numerical solution we seek a rank-r approximation in \mathcal{M} at every time step. The algorithm is consequently looking for a trajectory on the manifold \mathcal{M} that resembles the evolution guided by the equation. In some sense, we need to project the equation in $L^2(\Omega \times \mathcal{S}^{d-1})$ to the manifold and find the equation that governs the dynamics of this trajectory in \mathcal{M} .

We denote by u(t, x, v) the analytic solution and by $u_r(t, x, v)$ the numerical rankr approximation, then with the argument above, the governing equation for u_r is

(2.1)
$$\partial_t u_r = \mathcal{P}_{u_r}(\mathcal{L}u_r) = \mathcal{P}_{u_r}\left(\frac{\sigma(x)}{\epsilon^2}\left(\rho - u_r\right) - \frac{v}{\epsilon} \cdot \nabla_x u_r\right),\,$$

where $\mathcal{P}_u f$ stands for the projection of f onto the tangential plane of \mathcal{M} at u. Denoting $\mathcal{T}_{u_r} \mathcal{M}$ the tangential plane of \mathcal{M} at u_r , this projection operator ensures

$$\dot{u}_r \in \mathcal{T}_{u_r} \mathcal{M}$$
,

guaranteeing that u_r lies in the manifold \mathcal{M} for all time.

We now explicitly look for expression of the tangential plane and the projection operator. For a nonlinear manifold \mathcal{M} , such expressions necessarily depend on the point where the tangent is looked for. Denote

$$f = \sum_{ij} S_{ij} X_i V_j \in \operatorname{Span}\{X_i\}_{i=1}^r \otimes \operatorname{Span}\{V_j\}_{j=1}^r;$$

then the tangential plane is given by

$$\mathcal{T}_{f}\mathcal{M}$$

$$= \left\{ g \in L^{2}(\,\mathrm{d}x\,\mathrm{d}v) : g = \sum_{i,j=1}^{r} X_{i}(x) \dot{S}_{i,j} V_{j}(v) + \dot{X}_{i}(x) S_{i,j} V_{j}(v) + X_{i}(x) S_{i,j} \dot{V}_{j}(v) \right.$$
with $\dot{S} \in \mathbb{R}^{r \times r}, \dot{X}_{i} \in L^{2}(\Omega_{x}), \dot{V}_{j} \in L^{2}(\mathcal{S}^{d-1}), \text{and } \left\langle X_{i}, \dot{X}_{j} \right\rangle_{x} = \left\langle V_{i}, \dot{V}_{j} \right\rangle_{v} = 0 \right\}.$

This set collects all functions whose infinitesimal, when added to f, still yields a rank-r function. In this definition, we notice that we are allowed to choose arbitrarily an $r \times r$ matrix \dot{S} , a function list \dot{X}_i , and a function list \dot{V}_i , as long as the gauge conditions, $\langle X_i, \dot{X}_j \rangle_x = \langle V_i, \dot{V}_j \rangle_v = 0$, are satisfied. We note that the gauge conditions are imposed to guarantee the uniqueness of the low-rank factors. Interested readers are referred to [38] for details.

With this definition, one has

$$(2.2) \mathcal{P}_f q = \mathcal{P}_X q + \mathcal{P}_V q - \mathcal{P}_V \mathcal{P}_X q \quad \forall q \in L^2(\Omega_x \times \mathcal{S}^{d-1}),$$

where the spatial and velocity projection are

$$\mathcal{P}_X g = \sum_i^r \langle X_i, g \rangle_x X_i \,, \quad \mathcal{P}_V g = \sum_i^r \langle V_i, g \rangle_v V_i \,, \quad \mathcal{P}_V \mathcal{P}_X g = \sum_{i,j}^r X_i \langle X_i V_j, g \rangle_{x,v} V_j \,.$$

Inserting (2.2) into (2.1) gives us the governing equation for u_r :

(2.3)
$$\partial_t u_r = \mathcal{P}_{u_r}(\mathcal{L}u_r) = \left(\mathcal{P}_{X_{u_r}} + \mathcal{P}_{V_{u_r}} - \mathcal{P}_{V_{u_r}}\mathcal{P}_{X_{u_r}}\right)(\mathcal{L}u_r).$$

The numerical method will then be developed upon this formulation. We discuss the semidiscrete (in time) and the fully discrete schemes (both implicit Euler and CNIE) in detail in the following subsections.

2.1. Semidiscrete low-rank splitting method. In this section, we develop a projector splitting method to solve (2.3). In order to be concise, we simply denote the low-rank solution u_r by u and we decompose the solution using its low-rank representation:

(2.4)
$$u(t, x, v) = \sum_{i,j=1}^{r} X_i(t, x) S_{i,j}(t) V_j(t, v)$$
$$= X(t, x) S(t) V^{\top}(t, v) = X(t, x) L(t, v) = K(t, x) V^{\top}(t, v),$$

where X and V collects the basis functions

$$\begin{cases} X(t,x) = [X_1(t,x), X_2(t,x), \dots, X_r(t,x)], \\ V(t,v) = [V_1(t,v), V_2(t,v), \dots, V_r(t,v)]. \end{cases}$$

We will also be using quantities K and L:

(2.5)
$$L(t,v) = S(t)V^{\top}(t,v) = [L_1(t,v), L_2(t,v), \dots, L_r(t,v)]^{\top},$$

(2.6)
$$K(t,x) = X(t,x)S(t) = [K_1(t,x), K_2(t,x), \dots, K_r(t,x)].$$

Computing (2.3) at discrete times t_n amounts to finding the governing equations that provide the updates of

$$X^n$$
, V^n , and S^n ,

respectively, for all t_n with $n \geq 1$.

To specify the initial data, we project the initial condition onto \mathcal{M} using the singular value decomposition (SVD), namely,

(2.7)
$$u(t=0,x,v) \approx \sum_{i,j=1}^{r} X_i(t=0,x) S_{i,j}(t=0) V_j(t=0,v) = X^0(x) S^0(V^0(v))^T$$
.

For updating X, V, S, the Lie-Trotter splitting is used. From time step t_n to $t_{n+1} = t_n + \Delta t$, we split the three operators on the right-hand side of (2.3) into three substeps:

(2.8)
$$\partial_t u = \mathcal{P}_{X_u} \left(\frac{\sigma(x)}{\epsilon^2} \left(\rho - u \right) - \frac{v}{\epsilon} \cdot \nabla_x u \right),$$

(2.9)
$$\partial_t u = -\mathcal{P}_{\mathbf{V}_u} \mathcal{P}_{\mathbf{X}_u} \left(\frac{\sigma(x)}{\epsilon^2} \left(\rho - u \right) - \frac{v}{\epsilon} \cdot \nabla_x u \right),$$

(2.10)
$$\partial_t u = \mathcal{P}_{V_u} \left(\frac{\sigma(x)}{\epsilon^2} \left(\rho - u \right) - \frac{v}{\epsilon} \cdot \nabla_x u \right).$$

This splitting (2.8)–(2.10) takes place for each time step. That is, given the numerical solution at time t_n we update the solution to t_{n+1} by solving the three equations one after another. All equations are advanced for a full time step Δt . Different from directly solving (2.3), each substep only changes one part of the decomposition. In particular, the first splitting step (2.8) preserves X, the last (2.10) preserves V, and the middle step (2.9) merely updates S. This allows us to update the three components separately. Below we detail the evolution of each substep:

- Updating (2.8): Starting with $u^n(x,v) = \mathbf{X}^n(x)\mathbf{S}^n(\mathbf{V}^n(v))^{\top}$, we run (2.8) for a full time step Δt , and we denote the result by $u^{n+1/3}(x,v)$. The step preserves X and thus

$$X^{n+1/3}(x) = X^n(x).$$

To update $S^{n+1/3}$ and $V^{n+1/3}$, we plug the low-rank formulation (2.4) into (2.8) and obtain, for $1 \le i \le r$,

$$\partial_t L_i = -\frac{1}{\epsilon} \sum_{j=1}^r \left\langle X_i^n, v \cdot \nabla X_j^n \right\rangle_x L_j + \frac{1}{\epsilon^2} \sum_{j=1}^r \left\langle X_i^n, \sigma X_j^n \right\rangle_x \left(\langle L_j \rangle_v - L_j \right) ,$$

By using (2.5) we can simplify it to

$$(2.11) \qquad \partial_t \mathbf{L}(t,v) = -\frac{1}{\epsilon} \sum_{k=1}^d v_k \mathbf{A}_{\partial_k}^n \mathbf{L}(t,v) + \frac{1}{\epsilon^2} \mathbf{A}_{\sigma}^n \left(\langle \mathbf{L}(t,\cdot) \rangle_v - \mathbf{L}(t,v) \right),$$

where $v = [v_1, \dots, v_d]$, and $A_{\partial_k}^n$ and A_{σ}^n , both $\in \mathbb{R}^{r \times r}$, are matrix versions of the differential operator and the scattering operator, respectively:

(2.12)
$$\left[\mathbf{A}_{\partial_{k}}^{n} \right]_{i,j} = \left\langle X_{i}^{n}, \partial_{k} X_{j}^{n} \right\rangle_{x}, \ (1 \leq k \leq d),$$

$$\left[\mathbf{A}_{\sigma}^{n} \right]_{i,j} = \left\langle X_{i}^{n}, \sigma X_{j}^{n} \right\rangle_{x}.$$

We denote the solution of (2.11) by $L^{n+1/3}(v)$, and $S^{n+1/3}$ and $V^{n+1/3}(v)$ are obtained through the Gram–Schmidt process (QR factorization) which ensures the orthogonality of $V^{n+1/3}(v)$:

$$L^{n+1/3}(v) = S^{n+1/3} \left(V^{n+1/3}(v) \right)^{\top}.$$

Finally,

$$u^{n+1/3} = (XSV^{\top})^{n+1/3}$$
.

- Updating (2.9): In this step, (2.9) is evolved for Δt with initial condition $u^{n+1/3}$. Since the step only changes S, we immediately obtain

$$X^{n+2/3} = X^{n+1/3}$$
 and $Y^{n+2/3} = Y^{n+1/3}$.

Plugging the low-rank representation (2.4) into (2.9), we obtain, in matrix form,

(2.13)
$$\partial_t \mathbf{S}(t) = \frac{1}{\epsilon} \sum_{k=1}^d \mathbf{A}_{\partial_k}^n \mathbf{S}(t) \Xi_{v_k}^{n+2/3} - \frac{1}{\epsilon^2} \mathbf{A}_{\sigma}^n \mathbf{S}(t) \Gamma^{n+2/3},$$

where Ξ_{v_k} and Γ , both $\in \mathbb{R}^{r \times r}$, are the matrix versions of the multiplication operator associated to v_k $(1 \le k \le d)$ and the density term, respectively:

(2.14)
$$[\Xi_{v_k}]_{i,j} = \langle V_i(\cdot), (\cdot)_k V_j(\cdot) \rangle_v$$
 and $[\Gamma]_{i,j} = \langle V_i(\cdot) \rangle_v \langle V_j(\cdot) \rangle_v - \delta_{i,j}$.

We denote the computed update of (2.13) by $S^{n+2/3}$ and

$$u^{n+2/3} = (XSV^{\top})^{n+2/3}$$
.

- Updating (2.10): In this step, (2.10) is evolved for a full time step Δt with initial value $u^{n+2/3}$. This step preserves V. Thus,

$$V^{n+1}(v) = V^{n+2/3}(v) \implies \Xi^{n+1} = \Xi^{n+2/3} \text{ and } \Gamma^{n+1} = \Gamma^{n+2/3}$$

To update X^{n+1} and S^{n+1} , the low-rank formulation (2.4) is plugged into (2.8). In the matrix form we have

(2.15)
$$\partial_t \mathbf{K}(t,x) + \frac{1}{\epsilon} \sum_{k=1}^d \partial_k \mathbf{K}(t,x) \Xi_{v_k}^{n+1} = \frac{1}{\epsilon^2} \mathbf{K}(t,x) \Gamma^{n+1}.$$

Solving this equation we obtain $K^{n+1}(v)$, and the orthogonality of X^{n+1} is ensured through the Gram–Schmidt process:

$$K^{n+1}(x) = X^{n+1}S^{n+1}$$
.

With these three steps completed, one finally arrives at the numerical solution at time t_{n+1} ,

$$u^{n+1} = \left(\mathbf{X}\mathbf{S}\mathbf{V}^{\top}\right)^{n+1}$$

Remark 1. We describe the method without incorporating special boundary conditions. The problem is assumed to be a Cauchy problem with infinite boundary. In the numerical examples and the theorems that we prove below, we used periodic boundary condition to eliminate the possible complication induced by the boundary. If a Dirichlet-type boundary condition is provided, the incoming data may drive the solution away from the low-rank approximation, and a boundary layer that sees drastic changes in both x and v space is needed to damp the fluctuation. Recent analysis in this direction can be found in [50, 31, 32, 33] and the references therein.

2.2. Fully discrete low-rank splitting method. We discretize the aforementioned splitting method in time and phase space. We denote

(2.16)
$$\mathcal{X} = \{x_1, x_2, \dots, x_{N_x}\}, \quad \mathcal{V} = \{v_1, v_2, \dots, v_{N_y}\}$$

the sets of discrete points in Ω_x and \mathcal{S}^{d-1} . The discrete solution can then be represented as

$$\mathbb{R}^{N_x \times N_v} \ni u^n = \mathsf{X}^n \mathsf{S}^n (\mathsf{V}^n)^\top,$$

where $S^n = S^n$ and we abuse the notation by calling

(2.17)
$$X^n = [X_1^n \ X_2^n \ \dots \ X_r^n] \in \mathbb{R}^{N_x \times r}$$
 and $V^n = [V_1^n \ V_2^n \ \dots \ V_r^n] \in \mathbb{R}^{N_v \times r}$

with X_i^n and V_i^n denoting the *i*th mode evaluated at the grid points.

We now perform an implicit time integration of the three equations (2.11), (2.13), and (2.15) to overcome the stability issue introduced by the stiffness.

- For updating (2.11), $X^{n+1/3} = X^n$. Applying the implicit Euler scheme gives

(2.18)
$$\begin{cases} \frac{\mathsf{L}^{n+1/3} - \mathsf{L}^n}{\Delta t} + \frac{1}{\epsilon} \sum_{k=1}^d \mathsf{A}_{\partial_k}^n \mathsf{L}^{n+1/3} \mathsf{\Pi}_{v_k} = \frac{\mathsf{A}_{\sigma}^n}{\epsilon^2} \mathsf{L}^{n+1/3} \mathsf{C} \,, \\ \mathsf{QR} \text{ decomposition: } \mathsf{L}^{n+1/3} = \mathsf{S}^{n+1/3} (\mathsf{V}^{n+1})^\top \,, \end{cases}$$

or applying the Crank-Nicolson method (the first step of CNIE) gives

$$\begin{cases} \frac{\mathsf{L}^{n+1/3} - \mathsf{L}^n}{\Delta t} + \frac{1}{\epsilon} \sum_{k=1}^d \mathsf{A}_{\partial_k}^n \left(\frac{\mathsf{L}^{n+1/3} + \mathsf{L}^n}{2} \right) \mathsf{\Pi}_{v_k} = \frac{\mathsf{A}_{\sigma}^n}{\epsilon^2} \frac{\mathsf{L}^{n+1/3} + \mathsf{L}^n}{2} \mathsf{C} \,, \\ \mathsf{QR} \text{ decomposition: } \mathsf{L}^{n+1/3} = \mathsf{S}^{n+1/3} (\mathsf{V}^{n+1/3})^\top \,. \end{cases}$$

In the equation we have used

$$\mathbf{A}_{\partial_k}^n = (\mathbf{X}^n)^{\top} \mathsf{D}_k \mathbf{X}^n \,, \quad \mathbf{A}_{\sigma}^n = \mathbf{X}^{\top} \mathbf{\Sigma} \mathbf{X} \,,$$

$$(2.20) \qquad \qquad \mathsf{\Pi}_{v_k} = \mathrm{diag}(\mathcal{V}_k) \,, \quad \mathsf{C} = \frac{1}{N_v} e e^{\top} - \mathsf{I}_{N_v} \,,$$

with $e = (1, 1, ..., 1)^{\top}$. $\Sigma = \operatorname{diag}(\sigma(\mathcal{X}))$ is an $N_x \times N_x$ matrix with evaluations of σ at the grid points in \mathcal{X} assigned as diagonal entries and D_k is the discrete approximation of ∂_{x_k} . The specific form of D_k depends on the spatial discretization. We have used the simple rectangle rule for the integration in μ_v . This determines the form of C . Other numerical integral rules could also be applied and the specific form of C will change accordingly. Obviously $\mathsf{A}^n_{\partial_k}$ and A^n_{σ} are the discrete versions of (2.12).

- For updating (2.13), we note that X and V are preserved:

$$X^{n+2/3} = X^{n+1/3}$$
 and $V^{n+2/3} = V^{n+1/3}$

The direct application of the implicit Euler scheme gives

$$(2.21) \quad \frac{\mathsf{S}^{n+2/3} - \mathsf{S}^{n+1/3}}{\Delta t} - \frac{1}{\epsilon} \sum_{k=1}^d \mathsf{A}_{\partial_k}^n \mathsf{S}^{n+2/3} \Xi_{v_k}^{n+2/3} = -\frac{\mathsf{A}_{\sigma}^n}{\epsilon^2} \mathsf{S}^{n+2/3} \Gamma^{n+2/3} \,.$$

Similarly, if Crank–Nicolson (the second step of CNIE) is used , the scheme reads $\,$

(2.22)
$$\frac{\mathsf{S}^{n+2/3} - \mathsf{S}^{n+1/3}}{\Delta t} - \frac{1}{\epsilon} \sum_{k=1}^{d} \mathsf{A}_{\partial_{k}}^{n} \frac{\mathsf{S}^{n+2/3} + \mathsf{S}^{n+1/3}}{2} \Xi_{v_{k}}^{n+2/3} \\ = -\frac{\mathsf{A}_{\sigma}^{n}}{\epsilon^{2}} \frac{\mathsf{S}^{n+2/3} + \mathsf{S}^{n+1/3}}{2} \mathsf{\Gamma}^{n+2/3} \,.$$

Here $\Xi_{v_k}^{n+2/3}$ and $\Gamma^{n+2/3}$, both $r \times r$, are discrete versions of (2.14):

$$(2.23) \quad \Xi_{v_k}^{n+2/3} = (\mathsf{V}^{n+2/3})^\top \mathsf{\Pi}_{v_k} \mathsf{V}^{n+2/3} \,, \quad \mathsf{\Gamma}^{n+2/3} = (\mathsf{V}^{n+2/3})^\top \mathsf{C} \mathsf{V}^{n+2/3}$$

- Finally for updating (2.15), we note

$$V^{n+1} = V^{n+2/3}$$
, $\Gamma^{n+1} = \Gamma^{n+2/3}$, $\Xi^{n+1} = \Xi^{n+2/3}$

Defining

(2.24)
$$\mathsf{K}^{n+2/3} = \mathsf{X}^{n+2/3} \mathsf{S}^{n+2/3} ,$$

we apply the implicit Euler method for

(2.25)
$$\begin{cases} \frac{\mathsf{K}^{n+1} - \mathsf{K}^{n+2/3}}{\Delta t} + \frac{1}{\epsilon} \sum_{k=1}^{d} \mathsf{D}_{k} \mathsf{K}^{n+1} \Xi_{v_{k}}^{n+1} = \frac{\Sigma}{\epsilon^{2}} \mathsf{K}^{n+1} \mathsf{\Gamma}^{n+1} \,, \\ \mathsf{QR \ decomposition:} \ \mathsf{X}^{n+1} \mathsf{S}^{n+1} = \mathsf{K}^{n+1} \,. \end{cases}$$

The Crank–Nicolson method will not be used in the last step and thus we do not specify it.

We finalize the update for

$$u^{n+1} = X^{n+1}S^{n+1}(V^{n+1})^{\top}$$
.

We stress that the choice of D_k is not straightforward. Indeed, in the $\epsilon \to 0$ limit, a term $\mathsf{D}_k \Sigma^{-1} \mathsf{D}_k$ will appear as the discretization of the Laplacian term. To guarantee the self-adjointness on the discrete level, D_k needs to be specifically chosen. For more details see Remark 8.

We summarize the one-time step integrators in Algorithms 2.1 and 2.2.

Algorithm 2.1. One-time-step implicit Euler integrator

Input:

1. time step Δt ;

2. Input data: X^n , S^n , and V^n .

Run

- Construct $A_{\partial_k}^n$, A_{σ}^n by (2.20); Compute $L^n = S^n(V^n)^{\top}$;
- Update $L^{n+1/3}$ by solving (2.18) with Δt ;
- Perform QR decomposition to obtain $S^{n+1/3}$, V^{n+1} from (2.18); Construct $\Xi_{v_k}^{n+1}$ and Γ^{n+1} by (2.23);
- Update $S^{n+2/3}$ with Δt by solving (2.21);
- Construct $K^{n+2/3} = X^n S^{n+2/3}$ by (2.24);
- Update K^{n+1} with Δt by solving (2.25);
- Perform QR decomposition to obtain X^{n+1} , S^{n+1} from (2.25);

Output: Numerical solution X^{n+1} , S^{n+1} , V^{n+1} ;

Algorithm 2.2. One-time-step CNIE integrator

Input:

- 1. time step Δt ;
- 2. Input data: X^n , S^n , and V^n

\mathbf{Run}

- Construct $A_{\partial_k}^n$, A_{σ}^n by (2.20); Compute $L^n = S^n(V^n)^{\top}$;
- Update $L^{n+1/3}$ by solving (2.19) with Δt ;
- Perform QR decomposition to obtain $S^{n+1/3}$, V^{n+1} from (2.19); Construct $\Xi_{v_k}^{n+1}$ and Γ^{n+1} by (2.23);
- Update $S^{n+2/3}$ with Δt by solving (2.22);
- Construct $K^{n+2/3} = X^n S^{n+2/3}$ by (2.24);
- Update K^{n+1} with Δt by solving (2.25);
- Perform QR decomposition to obtain X^{n+1} , S^{n+1} from (2.25):

Output: Numerical solution X^{n+1} , S^{n+1} , V^{n+1} ;

- **3. Properties of the numerical scheme.** We investigate the properties of the numerical method in this section. In particular we will discuss the computational complexity and prove that the method captures the rank-1 structure in the parabolic regime.
- **3.1.** Computational complexity. To analyze the computational complexity is rather straightforward. Denote r the rank and N_x and N_v the cardinality of \mathcal{X} and \mathcal{V} , respectively. The matrices in the updating formula, X^n , S^n , V^n , are computed by solving (2.18), (2.21), (2.25). The cost is summarized in Table 1.

Because $r = O(1) \ll \min\{N_x, N_v\}$, in conclusion, we need $O(N_x^3 + N_v^3)$ flops per time step, instead of the $O(N_x^3 N_v^3)$ as required by the traditional solvers.

- **3.2.** Intuition of the error analysis. Before describing and proving our results in detail, in this section we first give a relatively vague justification on why the method works. As described in the introduction, there are two points we need to make:
 - Why does the true solution have an approximate low-rank structure? This question is rather fundamental and is independent of the method chosen: the rank structure of the solution purely depends on the governing PDE we are studying here.
 - Why does the method keep track of the low-rank structure? This question concerns the behavior of the specific method (dynamical low-rank approximation) we choose to use here.

Table 1

Floating point operation required for the dynamical low-rank algorithm. We note that in the computation of L^{n+1} , $S^{n+2/3}$, and K^{n+1} we used the classical LU decomposition. These steps can be sped up in implementation with iterative algorithms such as Krylov iteration. We leave out the discussion for this part of computational saving.

Operations	Floating point operations (flops)
Calculation of $A_{\partial_k}^n, A_{\sigma}^n$ (2.20)	$O(r^2N_x)$
Preparation of L^n	$O(r^2N_v)$
Total cost of preparation	$O(r^2(N_v + N_x))$
Calculation of $\Pi_{v_k} \otimes A^n_{\partial_k}$, $C \otimes A^n_{\sigma}$	$O(r^2N_v)$
Solving L^{n+1} (2.18)	$O(r^3N_v^3)$
Total cost of updating L	$O(r^3N_v^3)$
QR decomposition to obtain $S^{n+1/3}$, $V^{n+1/3}$	$O(r^2N_v)$
Calculation of $\Xi_{v_k}^{n+2/3}$ and $\Gamma^{n+2/3}$ (2.23)	$O(r^2N_v)$
Calculation of $\Xi_{v_k}^{n+2/3} \otimes A_{\partial_k}^n$, $\Gamma^{n+2/3} \otimes A_{\sigma}^n$	$O(r^3)$
Solving $S^{n+2/3}$ (2.22)	$O(r^6)$
Total cost of updating S	$O(r^6 + r^2 N_v)$
Preparation of $K^{n+2/3}$ (2.24)	$O(r^2N_x)$
Calculation of $\Xi_{v_k}^{n+2/3} \otimes D_k$, $\Gamma^{n+2/3} \otimes \Sigma$	$O(r^2N_x)$
Solving K^{n+1} (2.25)	$O(r^3N_x^3)$
Total cost of updating K	$O(r^3N_x^3)$
QR decomposition to obtain X^{n+1} , S^{n+1}	$O(r^2N_x)$
Total cost of one time step	$O(r^3(r^3 + N_v^3 + N_x^3))$

To answer the first question, we merely cite the following result.

THEOREM 3.1 (Theorem 2 of [2]). Denote u^{ϵ} the solution to the linear Boltzmann equation, for $(t, x, v) \in \mathbb{R}^+ \times \Omega_x \times \mathcal{S}^{d-1}$:

(3.1)
$$\partial_t u^{\epsilon} = \mathcal{L} u^{\epsilon} = \frac{\sigma}{\epsilon^2} \mathcal{L}_0 u^{\epsilon} + \frac{1}{\epsilon} \mathcal{L}_1 u^{\epsilon},$$

where $\mathcal{L}_0 u = \rho - u$ and $\mathcal{L}_1 u = -v \cdot \nabla_x u$. Then in the zero limit of ϵ , the solution converges to the solution of the diffusion equation $\partial_t \rho = \nabla_x \cdot \left(\frac{1}{d\sigma} \nabla_x \rho\right)$ in the sense that

$$||u^{\epsilon}(t,x,v) - \rho(t,x)||_{L_2(\operatorname{d} x \operatorname{d} \mu)} \le C\epsilon,$$

where C has no dependence on ϵ .

We note that periodic boundary conditions are imposed in the original theorem to avoid complications that may come from boundary layers. Essentially this theorem states that in the zero limit of ϵ , $u^{\epsilon}(t, x, v)$ loses its velocity dependence, and the dynamics will purely be reflected in the physical space. In some sense,

$$u^{\epsilon}(t, x, v) = \rho(x) + \mathcal{O}(\epsilon)$$

can be seen as the rank-1 approximation with the threshold set at any value bigger than ϵ .

The proof for the theorem uses the Hilbert expansion. Formally, one writes $u^{\epsilon} = u_0 + \epsilon u_1 + \epsilon^2 u_2 + \cdots$ and performs an asymptotic analysis. Showing Theorem 3.1 rigorously then amounts to bounding u_2 uniformly in ϵ (this exposition is rather lengthy and we omit it here).

To answer the second question amounts to proving that the dynamical low-rank approximation captures the rank structure of the solution. To do so, we recall

(3.2)
$$\partial_t u_r = \mathcal{P}_{u_r} \mathcal{L} u_r = \mathcal{P}_{u_r} \left[\frac{1}{\epsilon^2} \mathcal{L}_0 u_r + \frac{1}{\epsilon} \mathcal{L}_1 u_r \right].$$

Notice that the equation differs from its continuous counterpart (3.1) by the projection \mathcal{P}_{u_r} on the right-hand side. The key to the analysis is twofold:

- showing that the projection operator \mathcal{P}_{u_r} does not disturb the rank-1 structure of the solution;
- showing that upon the projection, the leading order of the numerical solution follows the correct dynamics.

To show the former, we mimic the analysis on the PDE level and perform the asymptotic analysis for (3.2) by setting $u_r = u_{r,0} + \epsilon u_{r,1} + \cdots$. Then in the leading order,

$$\mathcal{O}\left(\frac{1}{\epsilon^2}\right): \quad \mathcal{P}_{u_r}\mathcal{L}_0 u_{r,0} = 0.$$

Note that if we suppose $u_r \in \text{Span}\{X_i\} \otimes \text{Span}\{V_j\}$; then with the definition of \mathcal{L}_0 ,

$$\mathcal{L}_0 u_r = \rho - u_r = \langle u_r \rangle_v - u_r \in \operatorname{Span}\{X_i\} \otimes \operatorname{Span}\{V_j\} \quad \Rightarrow \quad \mathcal{P}_{u_r} \mathcal{L}_0 u_{r,0} = \mathcal{L}_0 u_{r,0} = 0.$$

This suggests that \mathcal{P}_{u_r} , at least in the leading order, does not induce new rank structure, and thus one has $u_{r,0} \in \text{Null}\mathcal{L}_0$, making u_r approximately rank 1. To show that $u_{r,0}$ follows the right equilibrium flow requires more delicate derivations in the higher order expansions, and we leave the details to section 3.

3.3. Asymptotic analysis of the implicit Euler method. To unify the notation, throughout this section, we denote by u^n a matrix of size $N_x \times N_v$ with u^n_{ij} being the numerical solution at t_n, x_i, v_j . Denote $e = [1, \dots, 1]^\top$ a column vector of length N_v and $e_n = e/\sqrt{N_v}$ the normalized version; then $\rho^n = u^n e$ is a vector of length N_x representing the discrete version of ρ at time t_n for spatial grid points \mathcal{X} . The hope is to show that density ρ^n solves (1.3) in the limit $\epsilon \to 0$.

Our first result concerns the behavior of the implicit Euler method in the asymptotic regime. The corresponding result, stated in Theorem 3.2, is shown under the following technical assumption.

Assumption 1. For all n, there exists an orthogonal matrix $Q^n \in \mathbb{R}^{r \times r}$ such that

(3.3)
$$V^{n,*} = V^n Q^n$$

$$= (e_n, \mathcal{V}_{1,n} + \epsilon a_1, \mathcal{V}_{2,n} + \epsilon a_2, \dots, \mathcal{V}_{d,n} + \epsilon a_d, V^*_{d+2}, \dots, V^*_r) + O(\epsilon^2),$$

where the components satisfy (for all $1 \le k \le d$ and $i \ge d + 2$)

(3.4)
$$e_{\mathbf{n}}^{\top} a_k = O(\epsilon), \ (\mathcal{V}_{k,\mathbf{n}})^{\top} V_i^{n+1,*} = O(\epsilon), \ e_{\mathbf{n}}^{\top} V_i^{n+1,*} = O(\epsilon^2).$$

Here $\mathcal{V}_i = [(v_1)_i, (v_2)_i, \dots (v_{N_v})_i]^{\top}$ collects the *i*th dimension component of all coordinates in \mathcal{V} . Since $v \in \mathbb{R}^d$, the subindex of \mathcal{V}_i changes from 1 to d. We further denote the normalization by $\mathcal{V}_{i,n} = \frac{\sqrt{d}}{\sqrt{N_v}} \mathcal{V}_i$.

Remark 2 (intuition of Assumption 1). To understand this assumption we link it to the proof for the diffusion limit in the continuous setting. For proving Theorem 3.1, it is expected that

$$u^{\epsilon} = u_0 + \epsilon u_1 + \epsilon^2 u_2 \,,$$

where u_0 has no v dependence and $u_1 \sim v \cdot \nabla_x u_0$. This means the leading order of the equation should be homogeneous in v and the next order linearly reflects v in every dimension. This is presented in the definition of $V^{n,*}$ where e_n and \mathcal{V}_i present homogeneity and linearity in the leading and the next order, respectively.

There are direct consequences of this assumption. Define $\alpha^n = (\mathsf{V}^n)^\top e_n$ and $\alpha^{n,*} = (\mathsf{V}^{n,*})^\top e_n$; then

(3.5)
$$\alpha^n = Q\alpha^{n,*}, \quad \alpha^{n,*} = (V^{n,*})^{\top} e_n = (1 + O(\epsilon^4), O(\epsilon^2), \dots, O(\epsilon^2))^{\top}.$$

Similarly, letting

$$\Xi^{n,*}_{v_k} = (\mathsf{V}^{n,*})^\top \Pi_{v_k} \mathsf{V}^n = \mathsf{Q}^\top \Xi^n_{v_k} \mathsf{Q} \quad \text{ and } \quad \mathsf{\Gamma}^{n,*} = (\mathsf{V}^{n,*})^\top \mathsf{C} \mathsf{V}^n = \mathsf{Q}^\top \mathsf{\Gamma}^n \mathsf{Q} = \mathsf{Q}^\top \mathsf{Q}^n \mathsf{Q}$$

we have for all $j \leq N_v$

(3.6)
$$\left(\Xi_{v_k}^{n,*}\right)_{1,j} = \left(\Xi_{v_k}^{n,*}\right)_{j,1} = \frac{1}{\sqrt{d}} \delta_{k+1,j} + O(\epsilon) ,$$

and some straightforward calculation gives

$$(3.7) \qquad (\alpha^n)^{\top} \Xi_{v_m}^n \Xi_{v_n}^n \alpha^n = (\alpha^{n,*})^{\top} \Xi_{v_m}^{n+1,*} \Xi_{v_n}^{n+1,*} \alpha^{n,*} = \frac{1}{d} \delta_{m,n} + O(\epsilon^2),$$

(3.8)
$$(\alpha^n)^{\top} \alpha^n = (\alpha^{n,*})^{\top} \alpha^{n,*} = 1 + O(\epsilon^4),$$

(3.9)
$$V^n \alpha^n = V^{n,*} \alpha^{n,*} = e_n + O(\epsilon^2),$$

$$(3.10) \qquad (\alpha^n)^{\top} \Gamma^n = (\alpha^{n,*})^{\top} \Gamma^{n,*} \mathbf{Q}^{\top} = O(\epsilon^2).$$

This assumption essentially says there are components in V^{n+1} that can represent e_n and all $\mathcal{V}_{k,n}$. It is a rather mild condition. Indeed, assuming the initial data has this form, then with small time step size, namely if $\Delta t \ll (\Delta x)^2$, the condition holds true at all later times, as explained in detail in Appendix B.

THEOREM 3.2. We employ the implicit Euler method to compute u^{n+1} from u^n , using (2.18), (2.21), and (2.25); then, under Assumption 1, there is a constant C independent of ϵ so that

$$||u^{n+1} - \rho_0^{n+1}e^{\top}||_2 \le C\epsilon$$
,

where ρ_0^{n+1} solves

(3.11)
$$\frac{\rho_0^{n+1} - \rho_0^{n+2/3}}{\Delta t} = \frac{1}{d} \sum_{k=1}^{d} \mathsf{D}_k \left(\mathsf{\Sigma}^{-1} \mathsf{D}_k \rho_0^{n+1} \right)$$

and $\|\rho_0^{n+2/3} - \rho_0^n\|_2 = O(\frac{(\Delta t)^2}{(\Delta x)^4})$. This means in the $\epsilon \to 0$ limit, the numerical solution is approximately rank 1, with the density solving the diffusion equation according to the implicit Euler method.

Remark 3 (the bad). We note that the implicit low-rank integrator based on the implicit Euler scheme has a strong requirement on Δt . It needs to be extremely small due to the $O(\frac{(\Delta t)^2}{(\Delta x)^4})$ error term. For example, even if we choose $\Delta t \propto (\Delta x)^4$ the error is only $\mathcal{O}(\Delta t)$ and we end up with a global error of order O(1). This renders this numerical method impractical for time integration.

Remark 4 (the good). The method is able to capture the correct low-rank structure. For $\epsilon \to 0$ we have $u^{n+1} = \rho_0^{n+1} e^{\top}$ approximately, meaning the solution has rank 1 and is a constant in v. This is precisely the analytic result derived for the diffusion limit, shown in Theorem 3.1.

Remark 5 (on the rigor of the proof). The proof we provide below for the theorem is formal in the sense that we use the Hilbert expansion without tracing the constant C's dependence on ϵ . This proof, however, can be made rigorous with C's dependence on ϵ explicitly removed. Essentially one follows the flow of the current structure of the proof and gives a bound at the second order expansion, as is done in the continuous setting [2]. It is significantly more tedious but provides little intuition, so we omit it from the current paper.

Proof. Throughout the proof, all quantities of interests will be expanded using the following ansatz, with the subindex standing for the level in the asymptotic expansion.

$$(3.12) p = p_0 + \epsilon p_1 + \epsilon^2 p_2 + \cdots.$$

We now proceed by performing the three steps in the low-rank projector splitting integrator.

Step 1. This step preserves X and updates L. Thus, we plug the asymptotic expansion of L into (2.18) and obtain

$$\begin{cases} O(1/\epsilon^2): & \mathsf{A}_\sigma^n \mathsf{L}_0^{n+1/3} \mathsf{C} = 0 \,, \\ O(1/\epsilon): & \sum_{k=1}^d \mathsf{A}_{\partial_k}^n \mathsf{L}_0^{n+1/3} \mathsf{\Pi}_{v_k} = \mathsf{A}_\sigma^n \mathsf{L}_1^{n+1/3} \mathsf{C} \,, \\ O(1): & \frac{\mathsf{L}_0^{n+1/3} - \mathsf{L}_0^n}{\Delta t} + \sum_{k=1}^d \mathsf{A}_{\partial_k}^n \mathsf{L}_1^{n+1/3} \mathsf{\Pi}_{v_k} = \mathsf{A}_\sigma^n \mathsf{L}_2^{n+1/3} \mathsf{C} \,. \end{cases}$$

Since A_{σ}^{n} is invertible, the equation for the leading order implies that $L_{0}^{n+1/3}$ lies in the null space of C^{\top} . According to (2.20) C is symmetric with null space span $\{e_{n}\}$. Immediately,

(3.14)
$$\mathsf{L}_0^{n+1/3} = l_0^{n+1/3} e_\mathrm{n}^\top \,,$$

where the $r \times 1$ vector $l_0^{n+1/3}$ is yet to be determined. Solving the $O(1/\epsilon)$ level equation for $\mathsf{L}_1^{n+1/3}$ we have

(3.15)
$$\mathsf{L}_{1}^{n+1/3} = -\sum_{k=1}^{d} (\mathsf{A}_{\sigma}^{n})^{-1} \mathsf{A}_{\partial_{k}}^{n} l_{0}^{n+1/3} e_{\mathbf{n}}^{\top} \mathsf{\Pi}_{v_{k}} + l_{1}^{n+1/3} e_{\mathbf{n}}^{\top},$$

where the term $l_1^{n+1/3}e_n^{\top}$ is an undetermined component lying in the null space of C. To close the system we consider the O(1) equation and multiply e_n on both sides:

$$\frac{\mathsf{L}_0^{n+1/3} e_{\mathrm{n}} - \mathsf{L}_0^{n} e_{\mathrm{n}}}{\Delta t} + \sum_{k=1}^{d} \mathsf{A}_{\partial_k}^n \mathsf{L}_1^{n+1/3} \mathsf{\Pi}_{v_k} e_{\mathrm{n}} = 0.$$

Plugging (3.15) into this equation and using

$$e_{\mathbf{n}}^{\mathsf{T}} \Pi_{v_{k_1}} \Pi_{v_{k_2}} e_{\mathbf{n}} = \frac{1}{d} \delta_{k_1, k_2} , \quad e_{\mathbf{n}}^{\mathsf{T}} \Pi_{v_k} e_{\mathbf{n}} = 0 ,$$

we obtain

$$\frac{l_0^{n+1/3} - \mathsf{L}_0^n e_{\mathbf{n}}}{\Delta t} - \frac{1}{d} \sum_{k=1}^d \mathsf{A}_{\partial_k}^n (\mathsf{A}_{\sigma}^n)^{-1} \mathsf{A}_{\partial_k}^n l_0^{n+1/3} = 0.$$

Considering $u_0^{n+1/3} = \mathsf{X}^n \mathsf{L}_0^{n+1/3} = \mathsf{X}^n l_0^{n+1/3} e_{\mathbf{n}}^{\top}$ and $\rho_0^{n+1/3} = u_0^{n+1/3} e_{\mathbf{n}} / \sqrt{N_v} = \mathsf{X}^n l_0^{n+1/3} / \sqrt{N_v}$, we obtain (using $\mathsf{X}^{\top} \mathsf{X} = \mathsf{I}$)

(3.16)
$$\frac{\rho_0^{n+1/3} - \rho_0^n}{\Delta t} - \frac{1}{d} \sum_{k=1}^d \mathsf{X}^n \mathsf{A}_{\partial_k}^n (\mathsf{A}_{\sigma}^n)^{-1} \mathsf{A}_{\partial_k}^n (\mathsf{X}^n)^\top \rho_0^{n+1/3} = 0.$$

Perform the QR decomposition of $L^{n+1/3}$ to obtain $V^{n+1/3}$ and $S^{n+1/3}$, and since V will not change in later steps, we have, also according to (2.23),

$$\begin{split} & \mathsf{V}^{n+1} = \mathsf{V}^{n+2/3} = \mathsf{V}^{n+1/3} \,, \\ & \Gamma^{n+1} = \Gamma^{n+2/3} = \Gamma^{n+1/3} = (\mathsf{V}^\top \mathsf{C} \mathsf{V})^{n+1/3} \,, \\ & \Xi^{n+1}_{v_k} = \Xi^{n+2/3}_{v_k} = \Xi^{n+1/3}_{v_k} = (\mathsf{V}^\top \Pi_{v_k} \mathsf{V})^{n+1/3} \,. \end{split}$$

For convenience, we use the superscript $(\cdot)^{n+1}$ uniformly for V, Γ, Ξ in the following discussion. According to Assumption 1, there is $Q \in \mathbb{R}^{r \times r}$ such that (3.3) holds true for $V^{n+1,*} = VQ$, then (3.7) holds true at the new time step.

Without loss of generality, in the following part of the proof, we ignore high order terms of ϵ .

Step 2. This step preserves X and V and updates S. We plug the asymptotic expansion of S into (2.21) to obtain

$$\begin{cases} O(1/\epsilon^2): & \mathsf{A}_\sigma^n \mathsf{S}_0^{n+2/3} \mathsf{\Gamma}^{n+1} = 0 \,, \\ O(1/\epsilon): & -\sum_{k=1}^d \mathsf{A}_{\partial_k}^n \mathsf{S}_0^{n+2/3} \Xi_{v_k}^{n+1} = -\mathsf{A}_\sigma^n \mathsf{S}_1^{n+2/3} \mathsf{\Gamma}^{n+1} \,, \\ O(1): & \frac{\mathsf{S}_0^{n+2/3} - \mathsf{S}_0^{n+1/3}}{\Delta t} - \sum_{k=1}^d \mathsf{A}_{\partial_k}^n \mathsf{S}_1^{n+2/3} \Xi_{v_k}^{n+1} = -\mathsf{A}_\sigma^0 \mathsf{S}_2^{n+2/3} \mathsf{\Gamma}^{n+1} \,. \end{cases}$$

Since A_{σ}^{n} is invertible, the leading order equation implies that $S_{0}^{n+2/3}$ lies in the null space of Γ^{n+1} . Thus, we have

(3.18)
$$\mathsf{S}_0^{n+2/3} = s_0^{n+2/3} (\alpha^{n+1})^\top,$$

where $s_0^{n+2/3} \in \mathbb{R}^{r \times 1}$ is yet to be determined.

We now follow the same strategy as in Step 1. That is, we plug the expression for $S_0^{n+2/3}$ into the equation of order $\mathcal{O}(1)$ and then project out the null space of Γ^{n+1} .

$$\mathsf{S}_1^{n+2/3} = -\sum_{k=1}^d (\mathsf{A}_\sigma^n)^{-1} \mathsf{A}_{\partial_k}^n \mathsf{S}_0^{n+2/3} \Xi_{v_k}^{n+1} + s_1^{n+2/3} (\alpha^{n+1})^\top.$$

Then we close the system by plugging the result for $S_1^{n+2/3}$ into the equation of order $\mathcal{O}(\epsilon)$. To do so, we first multiply α^{n+1} on both sides of the equation and use (3.10) for

$$\frac{\mathsf{S}_0^{n+2/3}\alpha^{n+1}-\mathsf{S}_0^{n+1/3}\alpha^{n+1}}{\Delta t} - \sum_{k=1}^d \mathsf{A}_{\partial_k}^n \mathsf{S}_1^{n+2/3} \Xi_{v_k}^{n+1}\alpha^{n+1} = 0 \,.$$

Noticing (3.18) and (3.7) we obtain

$$\frac{\mathsf{S}_0^{n+2/3}\alpha^{n+1}-\mathsf{S}_0^{n+1/3}\alpha^{n+1}}{\Delta t}+\frac{1}{d}\sum_{k=1}^d\mathsf{A}_{\partial_k}^n(\mathsf{A}_\sigma^n)^{-1}\mathsf{A}_{\partial_k}^ns_0^{n+2/3}=0\,.$$

Using (3.8), we obtain

$$(3.19) \qquad \frac{\mathsf{S}_0^{n+2/3}\alpha^{n+1} - \mathsf{S}_0^{n+1/3}\alpha^{n+1}}{\Delta t} + \frac{1}{d}\sum_{k=1}^d \mathsf{A}_{\partial_k}^n(\mathsf{A}_\sigma^n)^{-1}\mathsf{A}_{\partial_k}^n\mathsf{S}_0^{n+2/3}\alpha^{n+1} = 0.$$

Since we further have $V^{n+1}\alpha^{n+1} = e_n$ by (3.9), similar to (3.16), we finally obtain

(3.20)
$$\frac{\rho_0^{n+2/3} - \rho_0^{n+1/3}}{\Delta t} + \frac{1}{d} \sum_{k=1}^d \mathsf{X}^n \mathsf{A}^n_{\partial_k} (\mathsf{A}^n_\sigma)^{-1} \mathsf{A}^n_{\partial_k} (\mathsf{X}^n)^\top \rho_0^{n+2/3} = 0 \,,$$

where $\rho_0^{n+2/3} = \mathsf{X}_0^n \mathsf{S}_0^{n+2/3} (\mathsf{V}^{n+1})^\top e_n / \sqrt{N_v}$. We then update the leading order of K according to

(3.21)
$$\mathsf{K}_0^{n+2/3} = \mathsf{X}^n \mathsf{S}_0^{n+2/3} = \mathsf{X}^n s_0^{n+2/3} (\alpha^{n+1})^\top.$$

Step 3. This step preserves V and updates K. Thus, we plug the asymptotic expansion of K into (2.25) and obtain

(3.22)
$$\begin{cases} O(1/\epsilon^2) : & \Sigma \mathsf{K}_0^{n+1} \mathsf{\Gamma}^{n+1} = 0, \\ O(1/\epsilon) : & \sum_{k=1}^d \mathsf{D}_k \mathsf{K}_0^{n+1} \Xi_{v_k}^{n+1} = \Sigma \mathsf{K}_1^{n+1} \mathsf{\Gamma}^{n+1}, \\ O(1) : & \frac{\mathsf{K}_0^{n+1} - \mathsf{K}_0^{n+2/3}}{\Delta t} + \sum_{k=1}^d \mathsf{D}_k \mathsf{K}_1^{n+1} \Xi_{v_k}^{n+1} = \Sigma \mathsf{K}_2^{n+1} \mathsf{\Gamma}^{n+1}. \end{cases}$$

Since Σ is invertible, the leading order equation implies that K_0^{n+1} lies in the null space of Γ^{n+1} . Thus, we have

(3.23)
$$\mathsf{K}_0^{n+1} = k_0^{n+1} (\alpha^{n+1})^\top,$$

where $k_0^{n+1} \in \mathbb{R}^{N_x \times 1}$ is yet to be determined. We now follow the same strategy as in Steps 1 and 2, which is to plug the expression for K_0^{n+1} into the equation of order $\mathcal{O}(1)$ and then project out the null space of $\mathsf{\Gamma}^{n+1}$. Then we close the system by plugging the result for $\mathsf{K}_1^{n+2/3}$ into the equation of order $\mathcal{O}(\epsilon)$. This yields, once again using (3.7), (3.8), and (3.10),

(3.24)
$$\frac{\mathsf{K}_0^{n+1}\alpha^{n+1} - \mathsf{K}_0^{n+2/3}\alpha^{n+1}}{\Delta t} - \frac{1}{d} \sum_{k=1}^d \mathsf{D}_k \mathsf{\Sigma}^{-1} \mathsf{D}_k \mathsf{K}_0^{n+1}\alpha^{n+1} = 0.$$

Now, since $\rho_0^{n+1} = u_0^{n+1} e_n / \sqrt{N_v}$ and $u_0^{n+1} = \mathsf{K}_0^{n+1} \left(\mathsf{V}^{n+1}\right)^\top = k_0^{n+1} \alpha^\top \left(\mathsf{V}^{n+1}\right)^\top$, we obtain, by using (3.9),

(3.25)
$$\frac{\rho_0^{n+1} - \rho_0^{n+2/3}}{\Delta t} - \frac{1}{d} \sum_{k=1}^d \mathsf{D}_k \left(\mathsf{\Sigma}^{-1} \mathsf{D}_k \rho_0^{n+1} \right) = 0,$$

which concludes the proof for (3.11). To show $\|\rho_0^{n+2/3} - \rho_0^n\|_2 = O(\frac{(\Delta t)^2}{(\Delta x)^4})$, we denote $\mathcal{L} = \sum_{k=1}^d \mathsf{X}^n \mathsf{A}_{\partial_k}^n (\mathsf{A}_{\sigma}^n)^{-1} \mathsf{A}_{\partial_k}^n (\mathsf{X}^n)^{\top}$; then (3.16) and (3.20) can be written as

$$(3.26) \qquad \quad \rho_0^{n+2/3} = \left(\mathsf{I} + \frac{\Delta t}{d}\mathcal{L}\right)^{-1} \left(\mathsf{I} - \frac{\Delta t}{d}\mathcal{L}\right)^{-1} \rho_0^n = \left(\mathsf{I} - \frac{(\Delta t)^2}{d^2}\mathcal{L}^2\right)^{-1} \rho_0^n \,.$$

By using $(X^n)^{\top} X^n = I$ we can bound \mathcal{L} as follows:

$$\|\mathcal{L}\|_2 \le \frac{C_d}{(\Delta x)^2 \min(\sigma(x))}$$

with C_d being a constant depending on d only. Therefore,

$$\|\rho_0^{n+2/3} - \rho_0^n\|_2 = O\left(\frac{(\Delta t)^2}{(\Delta x)^4}\right) \quad \Rightarrow \quad \|\rho^{n+2/3} - \rho^n\|_2 = O\left(\frac{(\Delta t)^2}{(\Delta x)^4}\right) + O(\epsilon).$$

Finally, since

$$u_0^{n+1} = k_0^{n+1} \boldsymbol{\alpha}^\top \left(\mathsf{V}^{n+1} \right)^\top = k_0^{n+1} \left(e_{\mathbf{n}}^\top \mathsf{V}^{n+1} \right) \left(\mathsf{V}_0^{n+1} \right)^\top,$$

we follow that e_n lies in the span of $\mathsf{L}_0^{n+1/3}$ and thus in the span of $\mathsf{V}_0^{n+1} = \mathsf{V}_0^{n+1/3}$. We thus have $u_0^{n+1} = k_0^{n+1} e_n^{\mathsf{T}}$, as desired.

3.4. Asymptotic analysis of the CNIE scheme. As observed in the previous section, the implicit Euler has a strong requirement on Δt for the low-rank algorithm to preserve the rank structure. In Theorem 3.3 below, we will show that the symmetry in the first two steps of CNIE will bring the following advantage: the method can preserve the rank structure independent of the time step size Δt . However, we do assume well-prepared initial data.

THEOREM 3.3. Apply the CNIE method to compute u^{n+1} from u^n , using (2.19), (2.22), and (2.25). Assuming that $u^n = \rho_0^n e^\top + \mathcal{O}(\epsilon)$, and under Assumption 1, there is a constant C independent of ϵ so that

$$(3.27) ||u^{n+1} - \rho_0^{n+1} e^{\top}||_2 \le C\epsilon,$$

where

$$\frac{\rho_0^{n+1} - \rho_0^n}{\Delta t} - \frac{1}{d} \sum_{k=1}^d \mathsf{D}_k \left(\mathsf{\Sigma}^{-1} \mathsf{D}_k \rho_0^{n+1} \right) = 0 \,.$$

This means with well-prepared initial data, the limiting scheme is the implicit Euler method applied on the diffusion equation (1.3).

Remark 6 (the good). It is immediate that Theorem 3.3 differs from Theorem 3.2 in that we preserve ρ in the limit $\epsilon \to 0$ independent of the time step size. Note that both methods share the last step, which is responsible for propagating the diffusion equation.

Remark 7 (the bad). The CNIE based low-rank algorithm used here only "preserves" the asymptotic limit but is not able to drive the solution to the low-rank space. As stated in Theorem 3.3 we add the assumption that the initial value already has the corresponding structure of rank 1, up to an error of $\mathcal{O}(\epsilon)$, to ensure the initial data is well-prepared at each time step.

Remark 8 (the choice of D_k). We note that $D_k(\Sigma^{-1}D_k)$ may not be a self-adjoint operator in general if D_k is not chosen properly. In fact, if D_k is chosen as an upwind type, the discretization is a shifted diffusion by one grid point in space. If D_k is chosen as a central-scheme type, the self-adjoint property can be preserved, at the sacrifice of staggered behavior in the numerical solution. This type of problem is rather typical. A common way in the literature to overcome it is by introducing the even-odd decomposition; the even part goes to the limit and the odd part diminishes. The two components are evolved with different type of fluxes [35]. Here numerically we simply balance the two types with a correctly chosen weight so that central scheme plays the major role in the diffusion limit. We leave the possible extension of introducing even-odd decomposition to future research.

Proof. Most of the proof is very similar to the case of the implicit Euler scheme detailed in Theorem 3.2. Thus, we will only highlight the main differences here and refer the reader to the appendix for a more thorough exposition.

The asymptotic expansion for the first step is given by

$$\begin{cases} O(1/\epsilon): & \frac{1}{2}\mathsf{A}_{\sigma}^{n}\left(\mathsf{L}_{0}^{n+1/3}+\mathsf{L}_{0}^{n}\right)\mathsf{C}=0\,,\\ \\ O(1): & \frac{1}{2}\sum_{k=1}^{d}\mathsf{A}_{\partial_{k}}^{n}\left(\mathsf{L}_{0}^{n+1/3}+\mathsf{L}_{0}^{n}\right)\mathsf{\Pi}_{v_{k}}=\frac{1}{2}\mathsf{A}_{\sigma}^{n}\left(\mathsf{L}_{1}^{n+1/3}+\mathsf{L}_{1}^{n}\right)\mathsf{C}\,,\\ \\ O(\epsilon): & \frac{\mathsf{L}_{0}^{n+1/3}-\mathsf{L}_{0}^{n}}{\Delta t}+\frac{1}{2}\sum_{k=1}^{d}\mathsf{A}_{\partial_{k}}^{n}\left(\mathsf{L}_{1}^{n+1/3}+\mathsf{L}_{1}^{n}\right)\mathsf{\Pi}_{v_{k}}=\frac{1}{2}\mathsf{A}_{\sigma}^{n}\left(\mathsf{L}_{2}^{n+1/3}+\mathsf{L}_{2}^{n}\right)\mathsf{C}\,. \end{cases}$$

From the equation of order $\mathcal{O}(1/\epsilon)$, we only know that $\mathsf{L}_0^{n+1/3} + \mathsf{L}_0^n$ lies in the null space of C^{\top} ; we cannot make a similar claim for $\mathsf{L}_0^{n+1/3}$. However, from the assumption $u^n = \rho_0^n e^{\top} + \mathcal{O}(\epsilon)$ and from $u^n = \mathsf{X}^n \mathsf{L}^n$ we immediately obtain $\mathsf{L}_0^n = l_0^n e_n^{\top}$. This is an important ingredient in the remainder of the proof. It is also the first major difference between the present proof for the CNIE and the proof of Theorem 3.2, where this condition is automatically satisfied independent of the chosen initial value.

Using similar arguments as in the proof of Theorem 3.2 we can then show (see Lemma A.1 in the appendix for details)

- $L^{n+1/3}$ in (2.19) has the same form as (3.14),
- $S^{n+1/3}$ in (2.22) has the same form as (3.18), the equations for computing $u_0^{n+1/3}$ and $u_0^{n+2/3}$ ((A.10) and (A.11) in the appendix).

With further details given in Appendix A, we obtain

$$\begin{split} \rho_0^{n+1/3} &= \left(\mathsf{I} - \frac{(\Delta t)}{2d} \mathcal{L}^n\right)^{-1} \left(\mathsf{I} + \frac{(\Delta t)}{2d} \mathcal{L}^n\right) \rho_0^n, \\ \rho_0^{n+2/3} &= \left(\mathsf{I} + \frac{(\Delta t)}{2d} \mathcal{L}^n\right)^{-1} \left(\mathsf{I} - \frac{(\Delta t)}{2d} \mathcal{L}^n\right) \rho_0^{n+1/3}, \end{split}$$

where as before $\mathcal{L} = \sum_{k=1}^{d} \mathsf{X}^{n} \mathsf{A}_{\partial_{k}}^{n} (\mathsf{A}_{\sigma}^{n})^{-1} \mathsf{A}_{\partial_{k}}^{n} (\mathsf{X}^{n})^{\top}$. Combining these two equations we get $\rho_0^{n+2/3} = \rho_0^n$ for all n > 0, which is the desired result.

3.5. Summary. Viewing Theorems 3.2 and 3.3, it is clear that the implicit Euler method is able to capture the low-rank structure of the diffusion limit from arbitrary data at the cost of requiring a very small time step size, while the CNIE scheme preserves the rank structure of the well-prepared initial data without constraint on the time step size.

When we design algorithms, we should make use of the benefit of both. To do so, one can simply run the implicit Euler scheme with a Δt_1 that is small enough such that the error term $O\left((\Delta t_1)^2/(\Delta x)^4\right)$ is controlled to the desired accuracy. This time integrator, however, gets applied only once, and then in all subsequent time steps, i.e., all steps from time t_1 to time t_{max} , we apply the CNIE time integrator. Theorem 3.2 suggests that with the first step taken, all the prerequisites of Theorem 3.3 are already guaranteed, so the rank structure will be preserved along the propagation, as Theorem 3.3 suggests. In conclusion, for $\epsilon \to 0$, the numerical solution is rank 1 and homogeneous in velocity, with the density ρ satisfying the implicit Euler discretization of the diffusion equation (1.3).

We summarize the final method in Algorithm 3.1.

Algorithm 3.1. Dynamical low-rank splitting method for the linear Boltzmann equation.

Preparation:

- 1. Initial data: u(t = 0, x, v).
- 2. Input data: final time: t_{max} ; rank number: r; time step: $\Delta t_1 \leq \Delta t_2$. 3. Discretization points: $\mathcal{X} = \{x_1, x_2 \dots, x_{N_x}\}, \mathcal{V} = \{v_1, v_2 \dots, v_{N_v}\}$
- 4. Initialization: use SVD to construct initial u^0 such that (2.7):

$$u^{0} = \mathsf{X}^{0} \mathsf{S}^{0} (\mathsf{V}^{0})^{\top} \approx u(t = 0, x, v)$$

5. Construct Π_{v_k} , C by (2.20).

Run: set n=0;

call One-time-step implicit Euler integrator using Δt_1 to update X^1, S^1, V^1 , using Algorithm 2.1

While $t < t_{\text{max}}$: $n \to n+1$;

call One-time-step CNIE integrator using Δt_2 to obtain $\mathsf{X}^{n+1},\mathsf{S}^{n+1},\mathsf{V}^{n+1}$ using Algorithm 2.2.

Output: Numerical solution X^n , S^n , and V^n for $t_n \leq t_{\text{max}}$.

4. Numerical experiments. In this section we present some numerical evidence to showcase the property of the proposed dynamical low-rank integrator. Strictly speaking the linear Boltzmann equation is only defined for $d \geq 2$. However, in the quasi-two-dimensional case, assuming the data is homogeneous in the y-direction, the equation degenerates to a problem with one dimension in space. In this case the diffusion limit becomes

(4.1)
$$\partial_t u = \frac{1}{3} \partial_x \left(\sigma^{-1}(x) \partial_x u \right), \quad (t, x) \in \mathbb{R}^+ \times \Omega_x.$$

To measure the error we define

$$(4.2) \mathcal{P}_{x,l}^{error} = \|u - \mathsf{X}_l(\mathsf{X}_l)^\top u\|_F \quad \text{and} \quad \mathcal{P}_{v,l}^{error} = \|u - u\mathsf{V}_l(\mathsf{V}_l)^\top\|_F,$$

where u is the reference solution and X and V are the numerical solution computed using the dynamical low-rank integrator. The error is measured in the Frobenius norm for the matrix, which is equivalent to $L_2(dx d\mu_v)$ in the continuous version.

4.1. Projection error and singular value test. Before testing the dynamical low-rank numerical integrator, we first numerically justify that the solution is indeed of low rank. Setting the initial data to

$$f(0, x, v) = \begin{cases} 2, & 0.8 < x < 1.2, \\ 0 & \text{otherwise,} \end{cases}$$

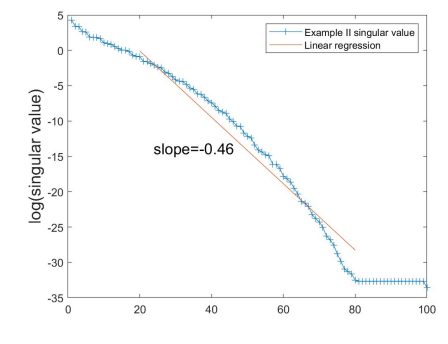
with the equation equipped with isotropic scattering and varying cross sections (see (4.6) and (4.7) below) at $\epsilon = 1$, we compute the equation with fine grids $(N_x = 200, N_v = 100, \text{ and } \Delta t = \Delta x/3)$ till $t_{\text{max}} = 1$. We plot the singular values of the solution in log-scale in Figure 1. It is clear that the singular values decay exponentially fast for both cases. This gives us the foundation to believe that the dynamical low-rank approximation would work.

4.2. Example I. We consider a toy problem with a constant scattering cross section

$$\sigma(x) = 2, \quad x \in [0, 2]$$

and the initial condition set as

(4.3)
$$f(0,x,v) = ((x-1)^2 + 1)(v^2 + 1).$$



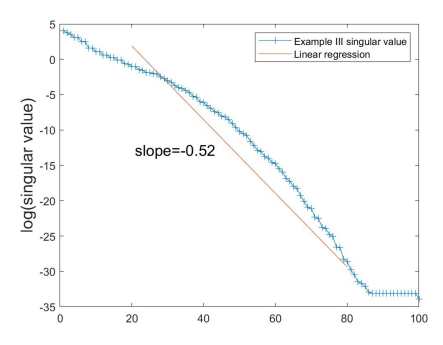


Fig. 1. Here we use $N_x=200$, $N_v=100$, $\Delta t=\Delta x/3$ and the direct implicit solver with upwind discretization for D to compute u. Left: Singular values of the solution u in Example II. Right: Singular values of the solution u in Example III.

In running Algorithm 3.1, the dynamical low-rank approximation, we combine central difference and upwind (CCP) flux for D, namely,

$$(4.4) \qquad (\mathsf{D}u^n)_{i,j} = \begin{cases} \epsilon \frac{u_i^n - u_{i-1}^n}{\Delta x} + (1 - \epsilon) \frac{u_{i+1}^n - u_{i-1}^n}{2\Delta x}, \ v_j > 0, \\ \epsilon \frac{u_{i+1}^n - u_i^n}{\Delta x} + (1 - \epsilon) \frac{u_{i+1}^n - u_{i-1}^n}{2\Delta x}, \ v_j \le 0. \end{cases}$$

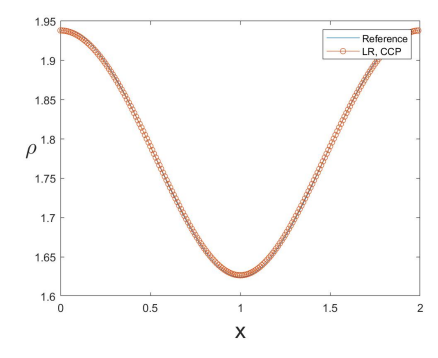
The combination factor is determined by the Knudsen number ϵ . This means in the kinetic regime when ϵ is close to 1 the flux becomes purely upwind but in the diffusion regime when $\epsilon \to 0$, the scheme is of central type. In the kinetic regime for $\epsilon = 1$, we set $N_x = 200$, $N_v = 100$, and $\Delta t = \Delta x/3$ for computing the reference solution, and we compare the low-rank integrator solution with r = 20 and the same (N_x, N_v) to this reference solution. Furthermore, $\Delta t_2 = \Delta x/3$ and $\Delta t_1 = (\Delta t_2)^2$. In the diffusion regime, for $\epsilon = 10^{-3}$, the reference solution is given by the numerical solution to the diffusion equation directly. Both cases are shown in Figure 2 (for $t_{\text{max}} = 1$ and $t_{\text{max}} = 0.1$, respectively), where we clearly see that the numerical solution matches the reference.

We realize the upwind flux typically brings high artificial diffusion, and this diffusion would be magnified in the diffusion equation when the flux term becomes stiff. To justify the choice of flux D defined above, here we compute the solution using a dynamical low-rank approximation with D simply set as the upwind type. The results are shown in Figure 3. For relatively big Knudsen number ($\epsilon = 1$), the low-rank integrator solution still agrees with the reference solution well, but the behavior significantly deteriorates in the diffusion regime when $\epsilon \to 0$. This is expected as stated in Remark 8 that the stencil for the upwind scheme is not symmetric, leading to the fact that D(Σ^{-1} D) is not a self-adjoint operator as it should be for the $\epsilon \to 0$ limit.

4.3. Example II. We consider the following initial condition:

(4.5)
$$f(0, x, v) = \begin{cases} 2, & 0.8 < x < 1.2, \\ 0 & \text{otherwise,} \end{cases}$$

and isotropic scattering with a cross section



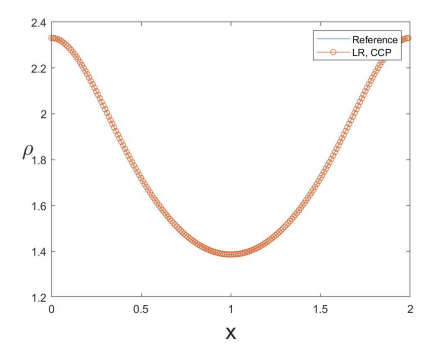
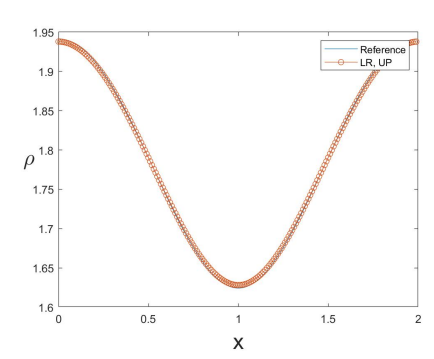


Fig. 2. Example I. We set $N_x = 200$, $N_v = 100$, $\Delta t = \Delta t_2 = \Delta x/3$, $\Delta t_1 = (\Delta t_2)^2$, r = 20. Left: $\epsilon = 1$, we compare the density ρ from the dynamical low-rank algorithm with a reference solution at $t_{max} = 1$. Right: $\epsilon = 10^{-3}$, we compare the density ρ from the dynamical low-rank algorithm with diffusion limit at $t_{max} = 0.1$.



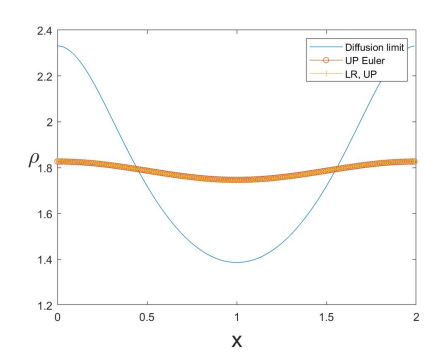
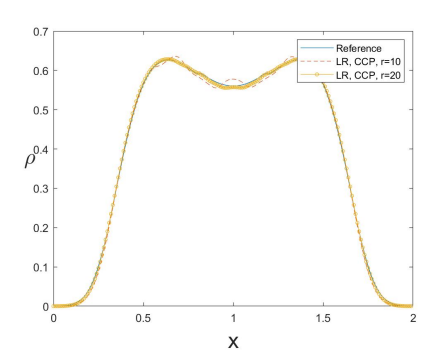


Fig. 3. Example I. $N_x=200, N_v=100, \Delta t=\Delta t_2=\Delta x/3, \Delta t_1=(\Delta t_2)^2, r=20$. Left: $\epsilon=1$, we compare the reference solution and the dynamical low-rank integrator solution with upwinding type of flux at $t_{max}=1$. Right: $\epsilon=10^{-3}$, we compare the solution to the diffusion equation with the dynamical low-rank integrator solution with upwinding type of flux at $t_{max}=0.1$. The D(Σ^{-1} D) term loses its symmetry, and the reference solution is not captured.



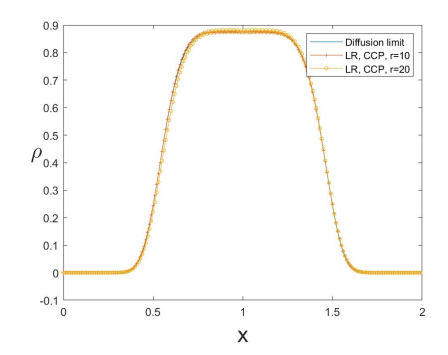


Fig. 4. Example II. $N_x=200, N_v=100, \Delta t=\Delta t_2=\Delta x/3, \Delta t_1=(\Delta t_2)^2$. Left: $\epsilon=1$ and r=10,20, we compare the density ρ from the low-rank algorithm using CCP for D_k with the implicit Euler/upwind solver at $t_{max}=1$. Right: $\epsilon=10^{-3}$ and r=10,20, we compare the density ρ from the low-rank algorithm using CCP with the diffusion limit at $t_{max}=0.1$. In the plots, LR stands for dynamical low-rank solution.

$$\sigma(x) = 100(x-1)^4.$$

The cross section thus becomes critical at x = 1. Comparing the dynamical low-rank solution using r = 20 to the reference solution (fine discretization for $\epsilon = 1$ and diffusion limit for $\epsilon = 10^{-3}$), we see good agreement, as shown in Figure 4. To be quantitative, we also plot the error, defined in (4.2), in Figure 5. It is clear that the error decays exponentially fast. We also test the dynamical low-rank integrator with D set to be of central scheme type. In this case, however, the method provides lots of artificial oscillation, as shown in Figure 6. These artificial oscillations do seem to capture the reference solution weakly (with oscillations centered around the true solution).

4.4. Example III. In the third example, we use the same initial condition as in Example II, but modify the cross section:

(4.7)
$$\sigma(x) = \begin{cases} 0.02, & x \in [0.35, 0.65] \cup [1.35, 1.65], \\ 1, & x \in [0, 0.35) \cup (0.65, 1.35) \cup (1.65, 2]. \end{cases}$$

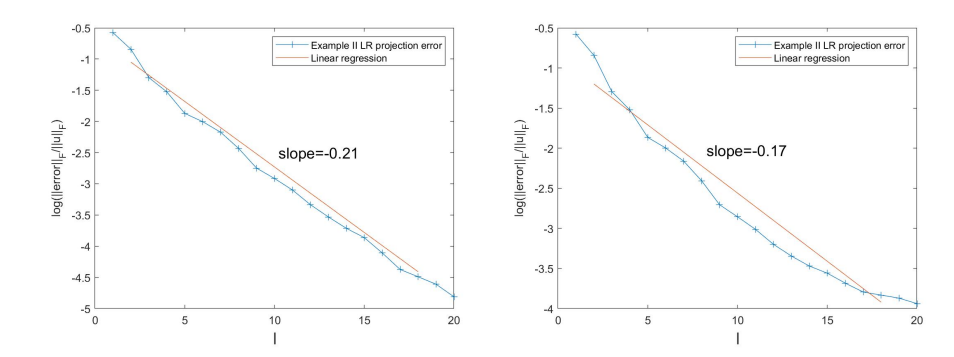


FIG. 5. Example II. $N_x = 200$, $N_v = 100$, $\Delta t = \Delta t_2 = \Delta x/3$, $\Delta t_1 = (\Delta t_2)^2$, r = 20. The numerical solution u is computed using the implicit Euler/upwind solver and X, V is computed using the low-rank algorithm. Left: $\log(\frac{\mathcal{P}_{x,l}^{error}}{\|u\|_F})$ as a function of l. Right: $\log(\frac{\mathcal{P}_{v,l}^{error}}{\|u\|_F})$ as a function of l.

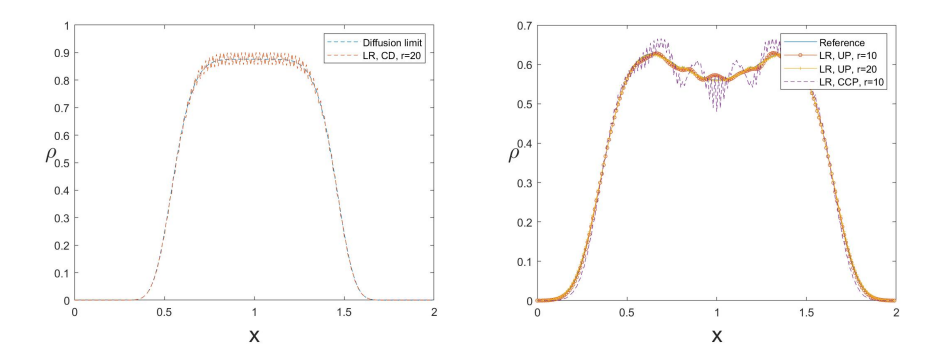


Fig. 6. Example II. $N_x=200, N_v=100, \Delta t=\Delta t_2=\Delta x/3, \Delta t_1=(\Delta t_2)^2$. Left: $\epsilon=1$ and r=10,20, we compare the density ρ from the low-rank algorithm using upwind and central differences for D_k with the implicit Euler/upwind solver at $t_{max}=1$. Right: $\epsilon=10^{-3}$ and r=20, we compare the density ρ from the low-rank algorithm using central differences with the diffusion limit at $t_{max}=0.1$. In the plots, LR stands for dynamical low-rank solution, and CS stands for central scheme, while UP stands for upwinding.

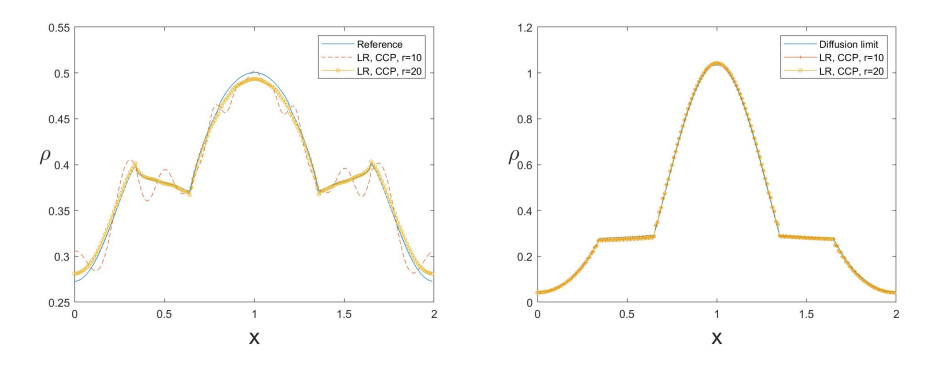
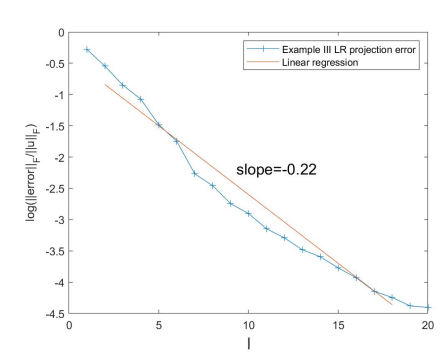


Fig. 7. Example III. $N_x=200, N_v=100, \Delta t=\Delta t_2=\Delta x/3, \Delta t_1=(\Delta t_2)^2$. Left: $\epsilon=1$ and r=10,20, we compare the density ρ from the low-rank algorithm using CCP for D_k with the implicit Euler/upwind solver at $t_{max}=1$. Right: $\epsilon=10^{-3}$ and r=10,20, we compare the density ρ from the low-rank algorithm using CCP with the diffusion limit at $t_{max}=0.1$.



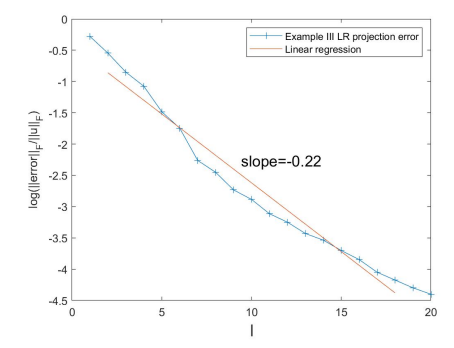


FIG. 8. Example III. Here we use $N_x = 200$, $N_v = 100$, $\Delta t = \Delta t_2 = \Delta x/3$, $\Delta t_1 = (\Delta t_2)^2$, r = 20. the numerical solution u is computed using the implicit Euler/upwind solver and X, V is computed using the low-rank algorithm. Left: $\log(\frac{\mathcal{P}_{v,l}^{error}}{\|u\|_F})$ as a function of l. Right: $\log(\frac{\mathcal{P}_{v,l}^{error}}{\|u\|_F})$ as a function of l.

This cross section is of high contrast and has a discontinuity, and thus the equation quickly achieves equilibrium in the optical thick region ($\sigma \sim 1$), while still staying in the kinetic regime in the optical thin region ($\sigma \sim 0.02$). The dynamical low-rank integrator uses r=20. To obtain the reference solutions, we either compute the equation with fine grid when $\epsilon=1$ or compute the diffusion equation directly with $\epsilon=10^{-3}$. We also compute the error: it decays exponentially fast, as plotted in Figure 8.

5. Conclusion. We have applied a projector splitting based dynamical low-rank approximation to a multiscale linear Boltzmann equation in diffusive scaling. Theoretically the equation has a low-rank structure in this regime, and this paper studies if the dynamical low-rank numerical method, a highly nonlinear numerical method, can capture such structure.

The result crucially depends on the employed time integrator. As shown above, if the implicit Euler method is employed, the time step size needs to be small. However, the CNIE method, due to its embedded symmetry, can preserve the low-rank structure automatically for mild time step size requirements, if the initial data is well-prepared. Combining these conclusions, we propose to run the Euler method for a very small time step size for merely one step to enforce the low-rank structure, and then switch to CNIE to preserve the rank structure. Numerical evidence is shown to agree well with the theoretical results obtained.

To our knowledge, this is the first analytical result on showing that the projectorsplitting dynamical low-rank approximation method truly preserves the rank structure in the kinetic framework.

Appendix A. Details for the proof of Theorem 3.3.

LEMMA A.1. If Assumption 1 holds true, then for all n > 0, L_0^n and $\mathsf{S}_0^{n+1/3}$ can be written as follows:

$$\mathsf{(A.1)} \qquad \quad \mathsf{L}_0^n = l_0^n e_{\mathrm{n}}^\top, \quad \mathsf{S}_0^{n+1/3} = s_0^{n+1/3} \left(\alpha^{n+1}\right)^\top, \quad \alpha^{n+1} = \mathsf{V}^{n+1} e_{\mathrm{n}}^\top,$$

with some $l_0^n \in \mathbb{R}^{r \times 1}$ and $s_0^{n+1/3} \in \mathbb{R}^{r \times 1}$.

Remark 9. Using Assumption 1 and Lemma A.1, we can further prove that in each step, $\mathsf{L}^{n+1/3}$ can be written as

(A.2)
$$\mathsf{L}^{n+1/3} = \hat{l}^{n+1/3} e_{\mathbf{n}}^{\top} - \epsilon \sum_{k=1}^{d} (A_{\sigma}^{n})^{-1} A_{\partial_{k}}^{n} \hat{l}^{n+1/3} e_{\mathbf{n}}^{\top} \Pi_{v_{k}} + O(\epsilon^{2}),$$

where $\hat{l}^{n+1/3} = l_0^{n+1/3} + \epsilon l_1^{n+1/3}$.

Proof. The proof proceeds by induction. First, for n = 1, by (3.23), after doing QR decomposition, we obtain

(A.3)
$$S_0^1 = s^1 e_{1,r}(\alpha^1)^\top, \quad e_{1,r} = (1,0,\dots,0)^\top \in \mathbb{R}^{r \times 1},$$

where $s^1 \in \mathbb{R}$ and $\alpha^1 = (\mathsf{V}^1)^\top e_n$. Using Assumption 1, we then get

(A.4)
$$\mathsf{L}_{0}^{1} = s^{1} e_{1,r}(\alpha^{1})^{\top} (\mathsf{V}^{1})^{\top} + O(\epsilon) = s^{1} e_{1,r}(\alpha^{1,*})^{\top} (\mathsf{V}^{1,*})^{\top} + O(\epsilon) = s^{1} e_{1,r} e_{\mathsf{n}}^{\top} + O(\epsilon).$$

Let $l_0^1 = s^1 e_{1,r}$; if we consider terms of order $O(1/\epsilon)$ in the asymptotic expansion of (2.19), we obtain

(A.5)
$$\mathsf{L}_0^{4/3} + \mathsf{L}_0^1 = l_0^{4/3} e_\mathrm{n}^\top + l_0^1 e_\mathrm{n}^\top.$$

After performing the QR decomposition we have

(A.6)
$$\mathsf{S}_0^{4/3} = \mathsf{L}_0^{n+1/3} \mathsf{V}^2 + O(\epsilon) = l_0^{4/3} e_n^\top \mathsf{V}^2 + O(\epsilon) = l_0^{4/3} \left(\alpha^2\right)^\top + O(\epsilon).$$

This shows that (A.1) holds true for n = 1.

Now if for n = k - 1, (A.1) holds true, then we can show that

$$\mathsf{L}_0^k = l_0^k e_\mathrm{n}^\top,$$

which implies

(A.8)
$$\mathsf{L}_0^{k+1/3} + \mathsf{L}_0^k = l_0^{k+1/3} e_{\mathrm{n}}^{\top} + l_0^k e_{\mathrm{n}}^{\top}.$$

Then we perform a QR decomposition and obtain

(A.9)
$$S_0^{k+1/3} = s_0^{k+1/3} \left(\alpha^{n+1}\right)^{\top},$$

where
$$s_0^{k+1/3} = l_0^{k+1/3}$$
.

We now consider the proof of Theorem 3.3 in more detail.

Proof. Steps 1–2. Instead of (3.16) and (3.20), we can obtain

(A.10)
$$\frac{u_0^{n+1/3}e - u_0^n e}{\Delta t} - \frac{1}{d} \sum_{k=1}^d \mathsf{X}^n \mathsf{A}^n_{\partial_k} (\mathsf{A}^n_\sigma)^{-1} \mathsf{A}^n_{\partial_k} (\mathsf{X}^n)^\top \frac{u_0^{n+1/3}e + u_0^n e}{2} = 0,$$

$$(\mathrm{A.11}) \quad \frac{u_0^{n+2/3}e - u_0^{n+1/3}e}{\Delta t} + \frac{1}{d} \sum_{k=1}^d \mathsf{X}^n \mathsf{A}^n_{\partial_k} (\mathsf{A}^n_\sigma)^{-1} \mathsf{A}^n_{\partial_k} (\mathsf{X}^n)^\top \frac{u_0^{n+2/3}e + u_0^{n+1/3}e}{2} = 0.$$

This gives us

(A.12)
$$\rho_0^{n+1/3} = \left(I - \frac{(\Delta t)}{2d} \mathcal{L}^n\right)^{-1} \left(I + \frac{(\Delta t)}{2d} \mathcal{L}^n\right) \rho_0^n,$$

(A.13)
$$\rho_0^{n+2/3} = \left(I + \frac{(\Delta t)}{2d} \mathcal{L}^n\right)^{-1} \left(I - \frac{(\Delta t)}{2d} \mathcal{L}^n\right) \rho_0^{n+1/3}$$

$$(A.14) \qquad \Rightarrow \rho_0^{n+2/3} = \rho_0^n.$$

Now, we obtain

(A.15)
$$\rho_0^{n+2/3} = \rho_0^n \quad \text{for } n > 0$$

in the first two splitting steps with the CNIE scheme.

Step 3. Using (A.1) we have

(A.16)
$$\mathsf{S}_0^{n+1/3} = s_0^{n+1/3} \left(\alpha^{n+1}\right)^\top.$$

From the terms of order $O(1/\epsilon)$ we then obtain

(A.17)
$$\mathsf{S}_0^{n+2/3} = s_0^{n+2/3} \left(\alpha^{n+1}\right)^{\top} \Rightarrow \mathsf{K}_0^{n+2/3} = k_0^{n+2/3} \left(\alpha^{n+1}\right)^{\top}.$$

Repeating the procedure used to derive (3.24)-(3.25), we still recover the diffusion limit in the last splitting step as

(A.18)
$$\frac{\rho_0^{n+1} - \rho_0^{n+2/3}}{\Delta t} - \frac{1}{d} \sum_{k=1}^{d} \mathsf{D}_k \left(\Sigma^{-1} \mathsf{D}_k \rho_0^{n+1} \right) = 0.$$

Appendix B. Discussion on the technical assumption. We first note that conditions (3.4), (3.5) in Assumption 1 guarantee the orthonormality of $V^{1,*}$. Now, using (3.5) and denoting $\alpha^{n+1,*} = \mathsf{Q}^{\top} \alpha^{n+1}$ we have

$$(B.1) \\ \alpha^{n+1,*}(\alpha^{n+1,*})^\top = \mathsf{Q}^\top \alpha^{n+1}(\alpha^{n+1})^\top \mathsf{Q}, \ (\alpha^{n+1,*})^\top \alpha^{n+1,*} = (\alpha^{n+1})^\top \alpha^{n+1} = 1 + O(\epsilon^4).$$

For each $1 \le k \le d$, we define

$$\Xi_{v_k}^{n+1,*} = (\mathsf{V}^{n+1,*})^\top \mathrm{diag}(\mathcal{V}_k) \mathsf{V}^{n+1,*};$$

then we get

$$\Xi_{v_k}^{n+1,*} = \mathsf{Q}^{\top} \Xi_{v_k}^{n+1} \mathsf{Q}, \quad (\Xi_{v_k}^{n+1,*})_{1,j} = (\Xi_{v_k}^{n+1,*})_{j,1} = \frac{1}{\sqrt{d}} \delta_{k+1,j} + O(\epsilon), \quad 1 \le j \le N_v,$$

where the second equality can be shown by using (3.5).

By considering (3.15) and (A.2), it suffices to show that the space spanned by the rows of

$$l_0^{n+1/3} e_{\mathrm{n}}^{\top} - \epsilon \sum_{i=1}^{d} (\mathsf{A}_{\sigma}^n)^{-1} \mathsf{A}_{\partial_i}^n l_0^{n+1/3} e_{\mathrm{n}}^{\top} \mathsf{\Pi}_{v_i}$$

can contain $e_n^{\top}, \mathcal{V}_1^{\top}, \dots, \mathcal{V}_d^{\top}$. This, in turn, is equivalent to showing that the following $\mathbb{R}^{r \times (d+1)}$ matrix has at least rank d+1:

(B.3)
$$\mathcal{R} = \left(\mathsf{A}_{\sigma}^{n} l_{0}^{n+1/3}, \mathsf{A}_{\partial_{1}}^{n} l_{0}^{n+1/3}, \dots, \mathsf{A}_{\partial_{d}}^{n} l_{0}^{n+1/3} \right).$$

For convenience, we only consider $\sigma(x) = 1$ and D_i is skew-symmetric.

First, we define the operator $\mathcal{H}: \mathbb{R}^{N_x \times 1} \to \mathbb{R}^{d \times d}$ as follows:

(B.4)
$$(\mathcal{H}(\mathbf{k}))_{i,j} = (\mathsf{D}_i \mathbf{k})^\top (\mathsf{D}_j \mathbf{k}), \quad \mathbf{k} \in \mathbb{R}^{N_x \times 1}.$$

LEMMA B.1. Assuming Assumption 1 is true for the numerical solution at time t_n , $\frac{\Delta t}{(\Delta x)^2}$ and ϵ are small enough, if

(B.5)
$$det(\mathcal{H}(k^n)) \neq 0,$$

where k^n is defined in (3.23), then Assumption 1 is true for the numerical solution at time t_{n+1} .

Remark 10. By Lemma B.1, we only need to check condition (B.5). Since k^n is a discrete approximation to $\rho(x,t^n)$, assume numerical error is small and the solution satisfies

$$D(\rho)(t) = \det\left(\int_{\Omega_x} \nabla \rho(x, t) \left(\nabla \rho(x, t)\right)^{\top} dx\right) \neq 0 \quad \forall 0 \leq t \leq T;$$

then we have $\mathcal{H}(k^n) \approx D(\rho)(t^n)$ and (B.5).

Proof. If Assumption 1 is true at time t_{n-1} , we have

$$\mathsf{K}^n = k^n \left(\alpha^n\right)^\top - \epsilon \sum_{i=1}^d \mathsf{D}_i k^n \left(\alpha^n\right)^\top \Xi_{v_i}^n + O(\epsilon^2)$$

and there exists an orthogonal matrix Q such that

(B.6)
$$\mathsf{K}^{n}\mathsf{Q} = k^{n} (\alpha^{n,*})^{\top} - \epsilon \sum_{i=1}^{d} \mathsf{D}_{i} k^{n} (\alpha^{n,*})^{\top} \Xi_{v_{i}}^{n,*} + O(\epsilon^{2}),$$

where $\alpha^{n,*}$, $\Xi_{v_i}^{n,*}$ satisfy (B.1) and (B.2).

Use (B.1) and (B.2), we can rewrite (B.6) as

(B.7)
$$\mathsf{K}^n \mathsf{Q} = \left(k^n, -\frac{\epsilon}{\sqrt{d}} \mathsf{D}_1 k^n, \dots, -\frac{\epsilon}{\sqrt{d}} \mathsf{D}_d k^n, \dots, \right) + O(\epsilon^2).$$

We notice that X^n comes from QR decomposition of K^{n-1} . Therefore, using (B.7), there exists an invertible matrix $P \in \mathbb{R}^{r \times r}$ such that

(B.8)
$$X^* = X^n P^{-1} = (k^n, -D_1 k^n, \dots, -D_d k^n, \dots) + O(\epsilon).$$

For any $1 \leq i \leq d$, we further define

(B.9)
$$\mathbf{A}_{\partial_i}^* = (\mathbf{X}^*)^\top \, \mathbf{D}_i \mathbf{X}^*, \text{ then } \mathbf{A}_{\partial_i}^n = \mathbf{P}^\top \mathbf{A}_{\partial_i}^* \mathbf{P}_i$$

and

(B.10)
$$\mathbf{A}_{\sigma}^{*} = (\mathbf{X}^{*})^{\top} \mathbf{\Sigma} \mathbf{X}^{*}, \text{ then } \mathbf{A}_{\sigma}^{n} = \mathbf{P}^{\top} \mathbf{A}_{\sigma}^{*} \mathbf{P}.$$

Plugging (B.9), (B.10) into (B.3) and defining $l^* = Pl_0^{n+1/3}$, it suffices to show that

$$\mathcal{R}^* = \left(\mathsf{A}_\sigma^* l^*, \mathsf{A}_{\partial_1}^* l^*, \dots, \mathsf{A}_{\partial_d}^* l^*\right)$$

has rank d+1. Now we divide the proof into two steps.

First step: $(l^*)_1 \gg 0$. Similar to (A.7), we have

$$\mathsf{S}^n \left(\mathsf{V}^n \right)^\top = \mathsf{L}^n = l_0^n e_{\mathrm{n}}^\top + O(\epsilon).$$

Using (3.3), (3.23), (B.1), we get

$$\mathsf{X}^*\mathsf{PS}^n\left(\mathsf{V}^n\right)^\top = \mathsf{K}^n\left(\mathsf{V}^n\right)^\top = k^n\left(\alpha^n\right)^\top\left(\mathsf{V}^n\right)^\top = k^n\left(\alpha^{n,*}\right)^\top\left(\mathsf{V}^{n,*}\right)^\top = k^ne_n^\top + O(\epsilon^2),$$

which implies

$$\mathsf{X}^*\mathsf{P}l_0^ne_{\mathbf{n}}^\top=k^ne_{\mathbf{n}}^\top.$$

Because X^* is an invertible matrix and the first column of X^* is k^n , we must have

(B.11)
$$(Pl_0^n)_1 = 1 + O(\epsilon).$$

Recalling that

(B.12)
$$(l^*)_1 = \left(\mathsf{P} l_0^{n+1/3}\right)_1,$$

similarly to asymptotic analysis performed to obtain (3.16), we have

$$\frac{\mathsf{L}_{0}^{n+1/3}e_{\mathrm{n}} - \mathsf{L}_{0}^{n}e_{\mathrm{n}}}{\Delta t} - \sum_{i=1}^{d} \mathsf{A}_{\partial_{i}}^{n} (\mathsf{A}_{\sigma}^{n})^{-1} \mathsf{A}_{\partial_{i}}^{n} \frac{l_{0}^{n+1/3} + l_{0}^{n}}{2} e_{\mathrm{n}}^{\mathsf{T}} \mathsf{\Pi}_{v_{i}}^{2} e_{\mathrm{n}} = 0$$

$$\Rightarrow \frac{l_{0}^{n+1/3} - l_{0}^{n}}{\Delta t} - \frac{1}{d} \sum_{i=1}^{d} \mathsf{A}_{\partial_{i}}^{n} (\mathsf{A}_{\sigma}^{n})^{-1} \mathsf{A}_{\partial_{i}}^{n} \frac{l_{0}^{n+1/3} + l_{0}^{n}}{2} = 0,$$

which implies

(B.13)
$$||l_0^{n+1/3} - l_0^n||_2 = O\left(\frac{\Delta t}{(\Delta x)^2}\right).$$

Combining (B.11), (B.12) with (B.13), we finally obtain

$$\left| \left(\mathsf{P} \left(l_0^{n+1/3} - l_0^n \right) \right)_1 \right| = O \left(\frac{\Delta t}{(\Delta x)^2} \right) + O(\epsilon) \Rightarrow (l^*)_1 > 1 - \left[O \left(\frac{\Delta t}{(\Delta x)^2} \right) + O(\epsilon) \right] \gg 0,$$

where $\frac{\Delta t}{(\Delta x)^2}$, ϵ have to be very small.

Second step: Γ^* is invertible. Now we can prove (B.5) by contradiction. Since D_i is skew-symmetric, and $A_{\partial_i}^*$ is skew-symmetric for each i, if we assume there exists $\gamma \in \mathbb{R}^{(d+1)\times 1}$ with $\|\gamma\|_2 = 1$ such that

(B.14)
$$\mathcal{R}^* \gamma = 0 \Rightarrow \left(\mathsf{A}_{\sigma}^* \gamma_1 + \sum_{i=i}^d \mathsf{A}_{\partial_i}^* \gamma_{i+1} \right) l^* = 0,$$

then, we deduce

$$(l^*)^{\top} \left(\mathsf{A}_{\sigma}^* \gamma_1 + \sum_{i=i}^d \mathsf{A}_{\partial_i}^* \gamma_{i+1} \right) l^* = 0 \Rightarrow \gamma_1 (l^*)^{\top} \mathsf{A}_{\sigma}^* l^* = 0$$
$$\Rightarrow \gamma_1 = 0 \Rightarrow \sum_{i=i}^d \mathsf{A}_{\partial_i}^* l^* \gamma_{i+1} = 0,$$

where we use $(l^*)^{\top} \mathsf{A}_{\partial_i}^* l^* = 0$.

Pluging (B.8) into (B.9), we obtain

(B.15)
$$\left(\mathsf{A}_{\partial_m}^*\right)_{i,j} = \begin{cases} \left(\mathsf{D}_{i-1}k^n\right)^\top \mathsf{D}_m \left(\mathsf{D}_{j-1}k^n\right), & 2 \leq i, j \leq d+1, \\ 0, & i = j, \\ -\left(\mathsf{D}_{i-1}k^n\right)^\top \left(\mathsf{D}_mk^n\right) + O(\epsilon), & 2 \leq i \leq d+1, \ j = 1, \end{cases}$$

for any $1 \leq m \leq d$. Consider the first column of $A_{\partial_i}^*$ from (B.15). Since $(l^*)_1 \gg 0$, (B.14) implies

$$\mathcal{H}(k^n)\gamma_{(2:d+1)} = 0,$$

where \mathcal{H} is defined in (B.4) and $\gamma_{(2:d+1)} \in \mathbb{R}^{d \times 1}$ is the cutoff vector to γ defined as

$$(\gamma_{(2:d+1)})_i = \gamma_{i+1}, \quad 1 \le i \le d.$$

Since $\mathcal{H}(k^n)$ is an invertible matrix, this finally shows that $\gamma_{(2:d+1)}$ has to be zero, which contradicts $\|\gamma\|_2 = 1$.

REFERENCES

- A. Arnold and T. Jahnke, On the approximation of high-dimensional differential equations in the hierarchical Tucker format, BIT, 54 (2014), pp. 305-341.
- [2] C. BARDOS, R. SANTOS, AND R. SENTIS, Diffusion approximation and computation of the critical size, Trans. Amer. Math. Soc., 284 (1984), pp. 617-649.
- [3] M. Bennoune, M. Lemou, and L. Mieussens, Uniformly stable numerical schemes for the Boltzmann equation preserving the compressible Navier-Stokes asymptotics, J. Comput. Phys., 227 (2008), pp. 3781–3803.
- [4] D. CONTE AND C. LUBICH, An error analysis of the multi-configuration time-dependent Hartree method of quantum dynamics, ESAIM Math. Model. Numer. Anal., 44 (2010), pp. 759–780.
- [5] N. CROUSEILLES, M. MEHRENBERGER, AND F. VECIL, Discontinuous Galerkin semi-Lagrangian method for Vlasov-Poisson, in ESAIM Proc. 32 (2011), pp. 211–230.
- [6] W. Dahmen, R. Devore, L. Grasedyck, and E. Süli, Tensor-sparsity of solutions to high-dimensional elliptic partial differential equations, Found. Comput. Math., 16 (2016), pd. 813–874.
- [7] P. DEGOND, F. DELUZET, L. NAVORET, A. SUN, AND M. VIGNAL, Asymptotic-preserving particle-in-cell method for the Vlasov-Poisson system near quasineutrality, J. Comput. Phys., 229 (2010), pp. 5630-5652.
- [8] P. Degond, S. Jin, and J. Liu, Mach-number uniform asymptotic-preserving gauge schemes for compressible flows, Bull. Inst. Math. Acad. Sin. (N.S.), 2 (2007).
- [9] G. DIMARCO AND L. PARESCHI, Exponential Runge-Kutta methods for stiff kinetic equations, SIAM J. Numer. Anal., 49 (2011), pp. 2057–2077.
- [10] G. DIMARCO AND L. PARESCHI, Numerical methods for kinetic equations, Acta Numer., 23 (2014), pp. 369–520.
- [11] L. EINKEMMER, A Low-Rank Algorithm for Weakly Compressible Flow, arXiv:1804.04561, 2018.
- [12] L. EINKEMMER, High performance computing aspects of a dimension independent semi-Lagrangian discontinuous Galerkin code, Comput. Phys. Commun., 202 (2016), pp. 326– 336.
- [13] L. EINKEMMER, A performance comparison of semi-Lagrangian discontinuous Galerkin and spline based Vlasov solvers in four dimensions, J. Comput. Phys., 376 (2019), pp. 937–951.
- [14] L. EINKEMMER AND C. LUBICH, A low-rank projector-splitting integrator for the Vlasov-Poisson equation, SIAM J. Sci. Comput., 40 (2018), pp. B1330-B1360.
- [15] L. EINKEMMER AND C. LUBICH, A quasi-conservative dynamical low-rank algorithm for the vlasov equation, SIAM J. Sci. Comput., 41 (2019), pp. B1061–B1081.
- [16] L. EINKEMMER, A. OSTERMANN, AND C. PIAZZOLA, A Low-Rank Projector-Splitting Integrator for the Vlasov-Maxwell Equations with Divergence Correction, arXiv:1902.00424, 2019.
- [17] F. FILBET AND E. SONNENDRÜCKER, Comparison of Eulerian Vlasov solvers, Comput. Phys. Commun., 150 (2003), pp. 247–266.

- [18] V. Grandgirard, J. Abiteboul, J. Bigot, T. Cartier-Michaud, N. Crouseilles, G. Dif-Pradalier, C. Ehrlacher, D. Esteve, X. Garbet, P. Ghendrih, G. Latu, M. Mehrenberger, C. Norscini, C. Passeron, F. Rozar, Y. Sarazin, E. Sonnendrücker, A. Strugarek, and D. Zarzoso, A 5D gyrokinetic full-f global semi-Lagrangian code for flux-driven ion turbulence simulations, Comput. Phys. Commun., 207 (2016), pp. 35–68.
- [19] J. HAEGEMAN, C. LUBICH, I. OSELEDETS, B. VANDEREYCKEN, AND F. VERSTRAETE, Unifying time evolution and optimization with matrix product states, Phys. Rev. B, 94 (2016), p. 165116.
- [20] J. Hu, S. Jin, and Q. Li, Asymptotic-preserving schemes for multiscale hyperbolic and kinetic equations, in Handbook of Numerical Methods for Hyperbolic Problems, R. Abgrall and C. Shu, eds., Handb. Numer. Anal. 18, Elsevier, Amsterdam, 2017, pp. 103–129.
- [21] S. Jin, Efficient asymptotic-preserving (AP) schemes for some multiscale kinetic equations, SIAM J. Sci. Comput., 21 (1999), pp. 441–454.
- [22] S. Jin and C. Levermore, Numerical schemes for hyperbolic conservation laws with stiff relaxation terms, J. Comput. Phys., 126 (1996), pp. 449–467.
- [23] S. JIN AND L. PARESCHI, Asymptotic-preserving (AP) schemes for multiscale kinetic equations: A unified approach, in Hyperbolic Problems: Theory, Numerics, Applications, H. Freistühler and G. Warnecke, eds., Birkhäuser Basel, Basel, 2001, pp. 573–582.
- [24] S. Jin, L. Pareschi, and G. Toscani, Uniformly accurate diffusive relaxation schemes for multiscale transport equations, SIAM J. Numer. Anal., 38 (2000), pp. 913–936.
- [25] E. KIERI, C. LUBICH, AND H. WALACH, Discretized dynamical low-rank approximation in the presence of small singular values, SIAM J. Numer. Anal., 54 (2016), pp. 1020–1038.
- [26] O. KOCH AND C. LUBICH, Dynamical low-rank approximation, SIAM J. Matrix Anal. Appl., 29 (2007), pp. 434–454.
- [27] O. KOCH AND C. LUBICH, Dynamical tensor approximation, SIAM J. Matrix Anal. Appl., 31 (2010), pp. 2360–2375.
- [28] K. KORMANN, A semi-Lagrangian Vlasov solver in tensor train format, SIAM J. Sci. Comput., 37 (2015), pp. 613–632.
- [29] E. LARSEN, J. MOREL, AND W. MILLER, Asymptotic solutions of numerical transport problems in optically thick, diffusive regimes, J. Comput. Phys., 69 (1987), pp. 283–324.
- [30] M. LEMOU AND L. MIEUSSENS, A new asymptotic preserving scheme based on micro-macro formulation for linear kinetic equations in the diffusion limit, SIAM J. Sci. Comput., 31 (2008), pp. 334–368.
- [31] Q. Li, J. Lu, And W. Sun, A convergent method for linear half-space kinetic equations, ESAIM Math. Model. Numer. Anal., 51 (2017), pp. 1583–1615.
- [32] Q. Li, J. Lu, and W. Sun, Half-space kinetic equations with general boundary conditions, Math. Comp., 86 (2017), pp. 1269-1301.
- [33] Q. Li, J. Lu, And W. Sun, Validity and regularization of classical half-space equations, J. Stat. Phys., 166 (2017), pp. 398–433.
- [34] Q. LI AND L. PARESCHI, Exponential Runge-Kutta for the inhomogeneous Boltzmann equations with high order of accuracy, J. Comput. Phys., 259 (2014), pp. 402–420.
- [35] Q. Li and L. Wang, Implicit asymptotic preserving method for linear transport equations, Commun. Comput. Phys., 22 (2017), pp. 157–181.
- [36] C. Lubich, From Quantum to Classical Molecular Dynamics: Reduced Models and Numerical Analysis, European Mathematical Society, Zürich, 2008.
- [37] C. Lubich, Time integration in the multiconfiguration time-dependent Hartree method of molecular quantum dynamics, Appl. Math. Res. Express AMREX, 2015 (2015), pp. 311–328.
- [38] C. Lubich and I. Oseledets, A projector-splitting integrator for dynamical low-rank approximation, BIT, 54 (2014), pp. 171–188.
- [39] C. Lubich, I. V. Oseledets, and B. Vandereycken, Time integration of tensor trains, SIAM J. Numer. Anal., 53 (2015), pp. 917–941.
- [40] C. Lubich, T. Rohwedder, R. Schneider, and B. Vandereycken, Dynamical approximation by hierarchical Tucker and tensor-train tensors, SIAM J. Matrix Anal. Appl., 34 (2013), pp. 470–494.
- [41] C. Lubich, B. Vandereycken, and H. Walach, Time integration of rank-constrained tucker tensors, SIAM J. Numer. Anal., 56 (2018), pp. 1273–1290.
- [42] H. MEYER, F. GATTI, AND G. A. WORTH, Multidimensional Quantum Dynamics, John Wiley & Sons, New York, 2009.
- [43] H. MEYER, U. MANTHE, AND L. S. CEDERBAUM, The multi-configurational time-dependent Hartree approach, Chem. Phys. Lett., 165 (1990), pp. 73–78.
- [44] C. MOUHOT AND C. VILLANI, On Landau damping, Acta Math., 207 (2011), pp. 29-201.

- [45] A. NONNENMACHER AND C. LUBICH, Dynamical low-rank approximation: Applications and numerical experiments, Math. Comput. Simul., 79 (2008), pp. 1346–1357.
- [46] A. OSTERMANN, C. PIAZZOLA, AND H. WALACH, Convergence of a low-rank Lie-Trotter splitting for stiff matrix differential equations, SIAM J. Numer. Anal., 57 (2019), pp. 1947–1966.
- [47] Z. Peng, Y. Chen, Y. Cheng, and F. Li, A Reduced Basis Method for Radiative Transfer Equation, arXiv/2103.07574, 2021.
- [48] N. J. SIRCOMBE AND T. D. ARBER, VALIS: A split-conservative scheme for the relativistic 2D Vlasov-Maxwell system, J. Comput. Phys., 228 (2009), pp. 4773-4788.
- [49] D. TER HAAR, Men of Physics: L.D. Landau, Vol. 2, Elsevier, Amsterdam, 1969.
- [50] L. Wu And Y. Guo, Geometric correction for diffusive expansion of steady neutron transport equation, Commun. Math. Phys., 336 (2015), pp. 1473–1553.